CrossMark

ORIGINAL PAPER

Evolution of the stress fields in the Zagros Foreland Folded Belt using focal mechanisms and kinematic analyses: the case of the Fars salient, Iran

Khalil Sarkarinejad[1] · Bahareh Zafarmand[1] · Behnam Oveisi[2]

Abstract The NW–SE trending Zagros orogenic belt was initiated during the convergence of the Afro–Arabian continent and the Iranian microcontinent in the Late Cretaceous. Ongoing convergence is confirmed by intense seismicity related to compressional stresses collision-related in the Zagros orogenic belt by reactivation of an early extensional faulting to latter compressional segmented strike–slip and dip–slip faulting. These activities are strongly related either to the deep-seated basement fault activities (deep-seated earthquakes) underlies the sedimentary cover or gently dipping shallow-seated décollement horizon of the rheological weak rocks of the infra-Cambrian Hormuz salt. The compressional stress regimes in the different units play an important role in controlling the stress conditions between the different units within the sedimentary cover and basement. A significant set of nearly N–S trending right-lateral strike–slip faults exists throughout the study area in the Fars area in the Zagros Foreland Folded Belt. Fault–slip and focal mechanism data were analyzed using the stress inversion method to reconstruct the paleo and recent stress conditions. The results suggest that the current direction of maximum principal stress averages N19°E, with N38°E that for the past from Cretaceous to Tertiary (although a few sites on the Kar-e-Bass fault yield a different direction). The results are consistent with the collision of the Afro–Arabian continent and the Iranian microcontinent. The difference between the current and paleo-stress directions indicates an anticlockwise rotation in the maximum principle stress direction over time. This difference resulted from changes in the continental convergence path, but was also influenced by the local structural evolution, including the lateral propagation of folds and the presence of several local décollement horizons that facilitated decoupling of the deformation between the basement and the sedimentary cover. The obliquity of the maximum compressional stress into the fault trends reveals a typical stress partitioning of thrust and strike–slip motion in the Kazerun, Kar-e-Bass, Sabz-Pushan, and Sarvestan fault zones that caused these fault zones behave as segmented strike–slip and dip–slip faults.

Keywords Fault–slip data · Earthquake focal mechanism · Paleo-stress · Recent tectonic stress · Zagros · Iran

✉ Bahareh Zafarmand
  bahar_zafarmand@yahoo.com

  Khalil Sarkarinejad
  sarkarinejad@susc.ac.ir

[1] Department of Earth Sciences, College of Sciences, Shiraz University, Shiraz, Iran

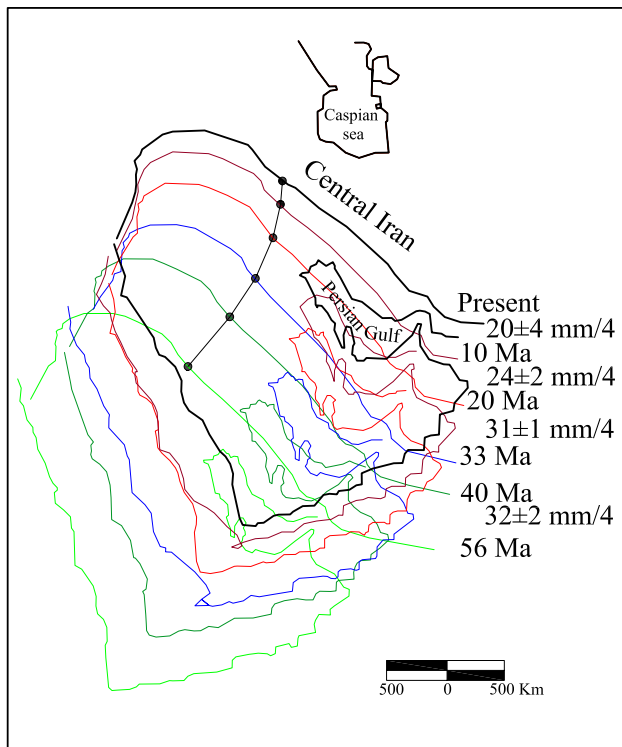[2] Geological Survey of Iran, Tehran, Iran

Introduction

The stratigraphy of the Zagros is well known because of its oil and gas potentials; however, critical questions remain about the relationship between the stress regime during the initiation of the Zagros orogenic belt and its later evolution. For example, as in some other collisional orogeny like Himalaya–Tibet orogeny, is the compressional direction almost parallel to the plate motion? What is the variation in the orientation of the principal stresses over time? Previous work (e.g., Vernant et al. 2004; McQuarrie et al. 2003) suggested that the convergence path between the Iranian microcontinent and the Afro–Arabian continent from the Mesozoic to the recent has been oblique and is deviated from N–E to N (Fig. 1). Is there data to support these proposed compressional trends over time? The deformation in the sedimentary

🖉 Springer

Fig. 1 Kinematic evolution paths of relative motion between the Afro–Arabian continent and the Eurasian continent since 56 Ma, to present (Simplified map from McQuarrie et al. 2003). Relative positions of Arabia with respect to Eurasia are shown as *black solid circles*. The reconstructions show the direction of Arabia–Eurasia motion changes from northeast to the north (McQuarrie et al. 2003). The average rate of convergence for each period of time is shown in the figure
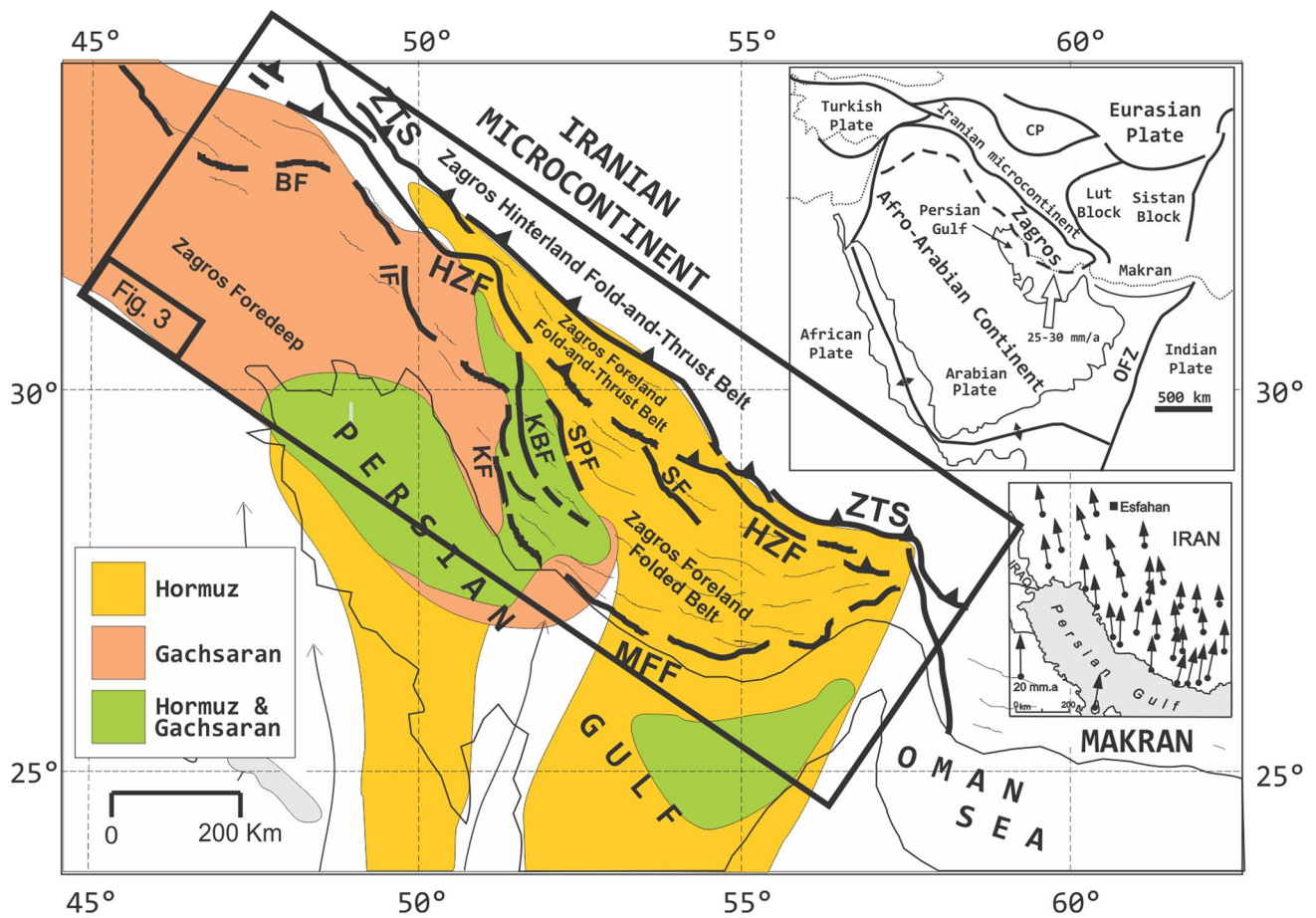
(McKenzie 1969; Angelier 2002; Otsubo et al. 2008). The paleo-stress analysis is referred by some authors as Angelier (1979, 1994), Yamaji (2000a, b), Zalohar and Vrabec (2007), and Misra et al. (2014) using the inverse problems. Inversion of earthquake focal mechanisms and fault–slip data is based on the Wallace–Bott hypothesis which assumes that striation slip occurs on each fault plane in the direction and sense of the maximum resolved shear stress. The traditional stress inversion approaches look for the best-fit stress tensor by minimizing or maximizing some object function which is defined through a summation of the compatibility functions for all fault–slip data (Zalohar and Vrabec 2007).

The Fars area is a key region to understand the tectonic and kinematic evolutions of the Zagros orogenic belt from the Cenozoic to the recent times. The study area is located in the central part of the Zagros Foreland Folded Belt (F-FOB) in the Fars salient (Fig. 3). To evaluate the possible stress variations along the trend of the orogeny from the northwest to the southeast, the study area extends from the Kazerun to Sarvestan fault zones (Fig. 3).

Tectonic and seismotectonic settings

The Zagros orogenic belt is the result of still continuing continent–continent collision between the Iranian microcontinent and the Afro–Arabian continent which probably started in the Late Cretaceous and developed during the Miocene–Pliocene times (Falcon 1974; Berberian and King 1981; Alavi 1994; Molinaro et al. 2005; Lacombe et al. 2006; Aubourg et al. 2010). The convergence of the Afro–Arabian continent with the Iranian microcontinent trends N–S to NNE, with a convergence velocity ranging from 23 (Bayer et al. 2003) to 35 mm year^{-1} (DeMets et al. 1990) (Fig. 2). The NE-trending shortening rate increases from the northwest to the southeast, up to approximately 10 mm year^{-1} (Tatar et al. 2002; Vernant et al. 2004). Some active transverse or cross faults within the Zagros orogenic belt, such as the Kazerun, Kar-e-Bass, Sabz-Pushan, and Sarvestan faults, trend nearly north–south, at a high angle to the structural trend of the orogenic belt, whereas other faults, such as the high Zagros and mountain front faults, trend NW–SE, sub-parallel to the belt. Right-lateral strike–slip faults cut across the trend of the belt and terminate as thrusts parallel to the folds (Figs. 2, 3). Folding, thrusting, and large-scale strike–slip transfer faulting is ongoing and seismicity is high in the area. The strike–slip faulting in the Zagros orogenic belt is comparable with such faulting from other collisional orogeny such as Himalaya (Mukherjee 2013, 2015a).

The high Zagros thrust fault divides the Zagros orogenic belt into two major belt-parallel structural zones known as the imbricated belt or high Zagros thrust belt in

cover is decoupled from the basement (likely at the level of the Hormuz salt). Is there any variation in the stress direction between the sedimentary cover and the upper gneissic crust? Unlike the locations of the studies by Lacombe et al. (2006) and Navabpour et al. (2007), the locations chosen in our study were close to fault zones. In the vicinity of the main lateral fault zones (e.g., Kazerun and Kar-e-Bass fault zones), is the stress regime similar to that in other parts of the Zagros orogenic belt? In other words, is there any significant deviation of compressional direction in the vicinity of the major lateral fault zone? This work will have a far reaching implication in seismicity of the Zagros orogenic belt.

In this study, we inferred the paleo and recent stress regimes based on the inversion of fault–slip data and earthquake focal mechanisms. We also used these results to test the role of the infra-Cambrian Hormuz salt (Mukherjee et al. 2010; Mukherjee 2011, 2013) as a décollement horizon between the sedimentary cover and the basement by comparing the results of the inversion of the fault–slip and earthquake focal mechanism data. Inversion of earthquake focal mechanisms has been proposed by several studies

Fig. 2 Structural map of the central Zagros orogenic belt showing geographic extent of the Gachsaran and Hormuz evaporitic facies (Sherkati and Letouzey 2004; Oveisi et al. 2009). *ZTS* Zagros thrust system, *HZF* high Zagros fault, *MFF* mountain front fault, *BF* Bala Rud fault zone, *IF* Izeh fault zone, *KF* Kazerun fault zone, *KSF* Kar-e-Bass fault zone, *SBZ* Sabz-Pushan fault zone, *SF* Sarvestan fault.

Upper right inset diagram shows the Afro–Arabian continent and the Iranian microcontinent. *White arrow* shows 25–30 mm/year motion of the Afro–Arabian continent relative to the Eurasian continent. *Lower right inset* shows GPS velocities (mm/yr) in the central Zagros with respect to stable Eurasia (Hessami et al. 2006). This map is modified from Sarkarinejad and Ghanbarian (2014)
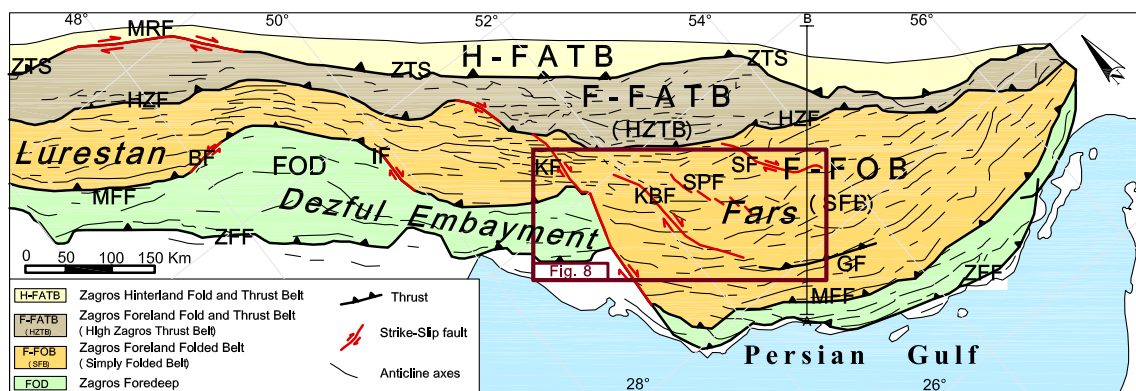
Fig. 3 Structural map and subdivision of the Iranian sector of the Zagros orogenic belt and location of the major fault zones including the study area (modified from Huber 1977; Berberian 1995; Sepehr and Cosgrove 2005; Sarkarinejad and Ghanbarian 2014; Sarkarinejad and Zafarmand 2017a, b). *H-FATB* Zagros hinterland fold-and-thrust belt, *F-FATB* Zagros foreland fold-and-thrust belt, *F-FOB* Zagros

Foreland Folded Belt, *FOD* Zagros foredeep, *ZTS* Zagros thrust system, *MRF* main recent fault, *HZF* high Zagros fault, *MFF* mountain front fault, *ZFF* Zagros foredeep fault, *BF* Balarud fault, *IF* Izeh fault, *KF* Kazerun fault, *KBF* Kar-e-Bass fault, *SPF* Sabz-Pushan fault, *SF* Sarvestan fault, *GF* Ghir fault. The AB *black line* indicates the cross-sectional path of Fig. 4

the northeast and the folded or simply folded belt in the southwest (Sepehr and Cosgrove 2005) (Fig. 3). Thrust faults and folds characterize the imbricated belt, whereas the simply folded belt has large, NW–SE-wards elongate anticlines. The mountain front fault subdivides the Foreland Folded Belt and has had a major role in controlling the sedimentation in the Zagros foreland basin since the early tertiary (Sepehr and Cosgrove 2004; Sherkati and Letouzey 2004). Based on the structural style and sedimentary history (Stöcklin 1968, 1974; Falcon 1974; Berberian and King 1981; Motiei 1993), the belt can be laterally divided into different zones: towards E—the Lurestan salient, the Dezful embayment, and the Fars salient (Sepehr and Cosgrove 2005; Lacombe et al. 2006) (Fig. 3).

As some authors (e.g., Sepehr and Cosgrove 2005; Burberry et al. 2011) suggested, Kazerun and Izeh faults are two pre-collisional faults in the Zagros orogenic belt that were initiated in the early Paleozoic as the extensional fault. It is suggested that during the early stages of plate collision (probably in oligocene, Aubourg et al. 2010), a gentle NW–SE trending within the Kazerun fault was initiated, and afterwards, this fault was reactivated as the segmented strike–slip and thrust fault. These lateral fault zones through the Zagros orogenic belt play a major kinematic role by accommodating the change in shortening, which is partitioned in the western central Zagros and non-partitioned in the eastern Zagros (Yamini-Fard et al. 2006, 2007). In the western central Zagros, the Afro–Arabia–Eurasia convergence is currently partitioned into NE–SW shortening that is perpendicular to the belt and right-lateral strike–slip faulting along the main recent fault (MRF) (Figs. 2, 3). In contrast, deformation in the eastern Zagros (Fars salient) is perpendicular to the local nearly E–W trends of the

belt (Talebian and Jackson 2004). This kinematic change requires extension along the strike of the belt, which is accommodated along the Kazerun–Borazjan, Kar-e-Bass, Sabz-Pushan, and Sarvestan faults (Talebian and Jackson 2004), which form a horsetail system that transfers and distributes orogen-parallel dextral slip along the MRF onto the thrusts and folds of the Zagros orogenic belt (Authemayou et al. 2005; Lacombe et al. 2006).

Sarkarinejad and Azizi (2008) divided the Zagros orogenic belt into seven major sub-parallel tectonic elements: 1—the Zagros simply folded belt; 2—the Zagros fold-and-thrust belt; 3—the Zagros thrust system (ZTS); 4—Zagros suture zone/ophiolite zone; 5—the Sanandaj–Sirjan HP–LT metamorphic belt; 6—the Sanandaj–Sirjan HT–LP metamorphic belt; and 7—the Urumieh–Dokhtar magmatic belt. Sarkarinejad and Ghanbarian (2014) introduced new terminology that relates to orogenic belt and the Zagros hinterland fold-and-thrust belt (H-FATB). They suggested that the Zagros orogenic belt could be divided into seven major belts. In this paper, we modified these divisions and introduce the new division that divides Zagros orogenic belt into nine sub-parallel tectonic belts; these include from SW to NE: 1—Zagros Foreland Folded Belt; 2—Zagros foreland fold-and-thrust belt; 3—Zagros thrust system; 4—Zagros suture zone/ophiolite zone; 5—slate belt; 6—Zagros hinterland fold-and-thrust belt; 7—Sanandaj–Sirjan HP–LT metamorphic belt; 8—HT–LP metamorphic belt; and 9—Urumieh–Dokhtar magmatic belt (Fig. 4).

From the Cambrian to the Early Cretaceous, the Zagros orogenic belt experienced a long period of relatively stable platform sedimentation (Stampfli and Borel 2002; Sepehr and Cosgrove 2005). After the convergence began in probably the Late Cretaceous, the Pabdeh neritic marls and shale

Fig. 4 Crustal-scale cross section of the Zagros orogenic belt (divisions are modified from Sarkarinejad and Azizi 2008; Sarkarinejad and Ghanbarian 2014); from SW to NE: (1) Zagros Foreland Folded Belt; (2) Zagros foreland fold-and-thrust belt; (3) Zagros thrust system (ZTS); (4) Zagros suture zone/ophiolite zone; (5) slate belt; (6) Zagros hinterland fold-and-thrust belt; (7) Sanandaj–Sirjan HP–LT metamorphic belt; (8) Sanandaj–Sirjan HT–LP metamorphic belt; and (9) Urumieh–Dokhtar magmatic belt
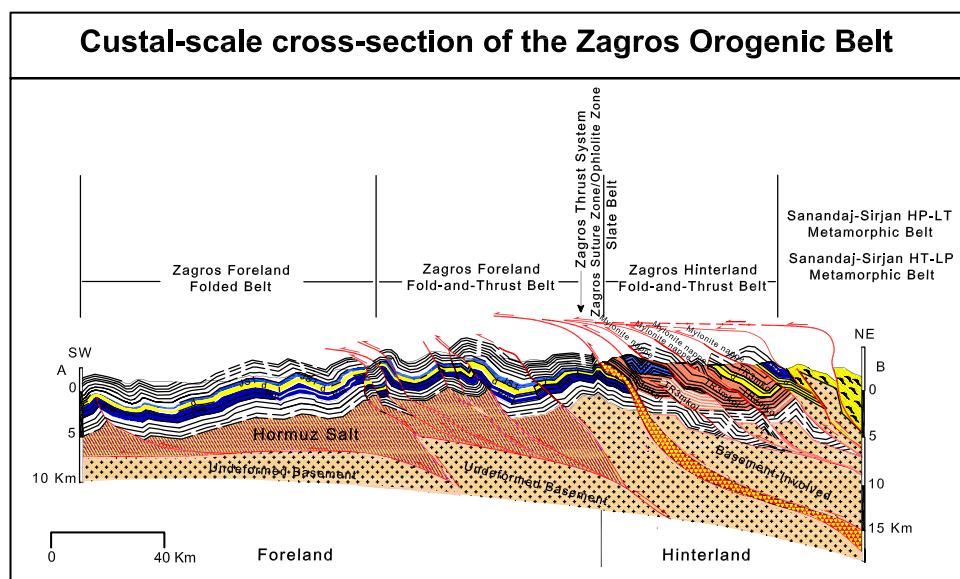
deposited in the Fars area. During the oligocene, Asmari massive shallow marine carbonates were deposited above the Pabdeh formation in the southwest, and the Jahrom formation was unconformably deposited in the northeast. From the Miocene to the Pliocene, the Fars group (which includes the Gachsaran, Mishan, and Agha Jari formation) deposited over the Asmari formation. These formations reflect the progressive infilling of the Zagros foreland basin (Lacombe et al. 2006) (Fig. 5). During the Pliocene, the continental Bakhtiari conglomerates represent the last main stage of sedimentation and are conformable along the Zagros front, but are unconformable in other parts of the belt to the northeast (Falcon 1961; Hessami et al. 2001; Homke et al. 2004) (Fig. 5).

The infra-Cambrian Hormuz salt in the Fars area lies on top of the basement and served as the major décollement horizon during the Late Tertiary deformation. Other décollement horizons include the Triassic Dashtak formation (evaporites), the Cretaceous Kazhdumi formation (shale), and the lower Miocene Gachsaran formation (evaporites) (Fig. 5). These décollement horizons decoupled deformation between the basement and sedimentary cover and also between different units within the sedimentary cover. These horizons control the pattern and distribution of deformation within the Zagros (O'brien 1950; Colman 1978; Letouzey and Sherkati 2004; Sepehr and Cosgrove 2004; Casciello et al. 2009; Farzipour-Saein et al. 2009). The GPS-derived velocity field and the seismicity record show decadal-scale quiescence across the higher elevation parts of the Zagros and confirm the absence of active upper crustal shortening within this region (Allen et al. 2013).

In the Zagros orogenic belt, the faults formed before, during, or after folding. Pre-folding faults include syn-sedimentary normal faults and small-scale thrusts (Casini et al. 2011; Lacombe et al. 2011). Thrust faults, that have the vergence to SW, developed during folding, and strike–slip faults typically postdate the pre- and syn-folding structures and probably relate to the later stages of fold tightening. The general chronology of the brittle tectonic events, with the corresponding σ_1 (maximum principal stress axis) trend within the Zagros, from previous studies (e.g., Navabpour et al. 2007 within the high Zagros belt in Fars Province) is NE–SW, NNE–SSW, NW–SE, and N–S. FL refers to the main stage of folding and related reverse structures, and it occurred between the NE and NNE events. The sequence of NE → FL → NNE → N indicates an anticlockwise rotation in the compression direction over time. Due to the lack of a sufficient number of compatible chronologies, Navabpour et al. (2007) noted that the geochronology of the NW event is not reliably constrained with respect to the other events.

The seismicity in the Zagros orogenic belt is limited to the region between the Persian Gulf coastal plain and the Zagros thrust system (Fig. 6). The abundance of earthquakes in this region indicates that the area is actively
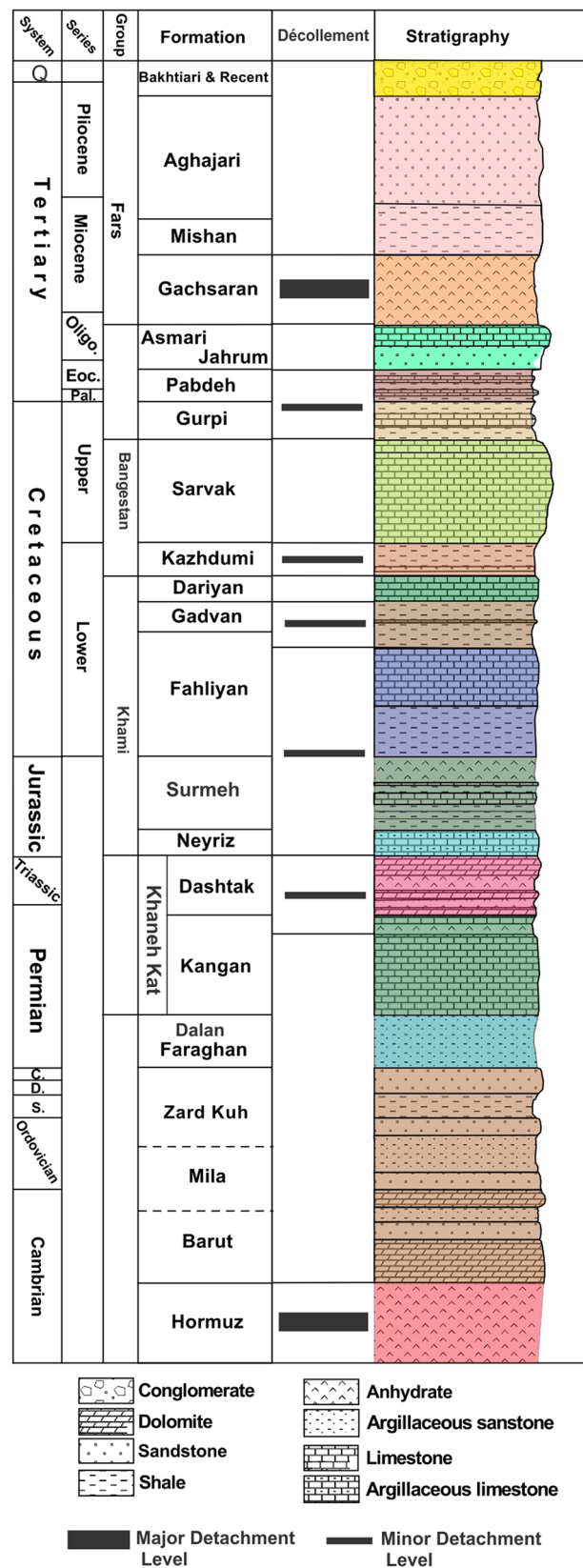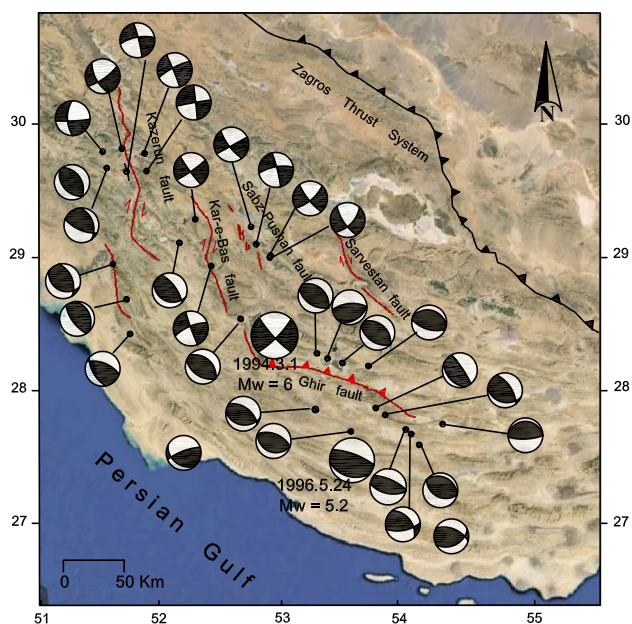

Fig. 5 Stratigraphic column of the Zagros Foreland Folded Belt (F-FOB). *Heavy black lines* indicate possible décollement levels within the sedimentary succession

Fig. 6 Focal mechanisms of moderate earthquakes reported by Talebian and Jackson (2004); modified from Lacombe et al. (2006). Most of the thrust earthquakes occur along the SW Zagros margin, between the coastal plain of the Persian Gulf and the Ghir thrust system, while strike–slip earthquakes are closely associated with the Kazerun, Kar-e-Bass, and Sabz-Pushan faults

deforming, a kind of out-of-sequence deformation that has also been noted from similar collisional orogeny (e.g., Mukherjee et al. 2012). The larger magnitude earthquakes ($M_b > 5$) are concentrated in the Zagros Foreland Folded Belt, an area of low topography (<1500–2000 m; Jackson and McKenzie 1984; Ni and Barazangi 1986; Talebian and Jackson 2004; Hatzfeld et al. 2010). Tatar et al. (2004) and Hatzfeld et al. (2010) infer that the seismicity in the central Zagros is beneath the sedimentary cover and within the upper part of the basement (between ~10 and ~15 km depth) (Figs. 7, 8). These earthquakes are not located on the main faults, as observed at the surface, but instead are spread over more distributed areas (Hatzfeld et al. 2010). Furthermore, the presence of Hormuz salt at the base of the ~10 km-thick folded sedimentary cover, together with the general absence of coseismic surface rupturing, indicates that earthquakes are concentrated within the basement (Nissen et al. 2011).

Catalogues of earthquakes determined earthquake locations in this region with uncertainties of up to 50 km in map view (Maggi et al. 2000; Ambraseys 2001; Talebian and Jackson 2004; Lohman and Simons 2005).

Yamini-Fard et al. (2006, 2007) analyzed the focal mechanisms and found that at the intersection between the Kazerun fault and the MRF in Borujen, as well as at the transition between the Zagros collision zone and the Makran subduction zone near Bandar Abbas, the thrust focal mechanisms
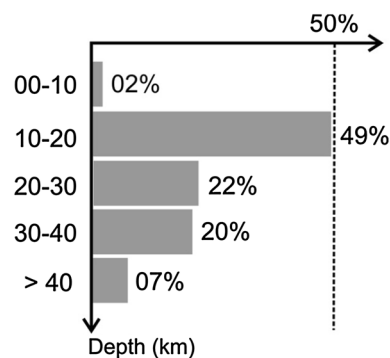
Fig. 7 Diagram of focal depth abundances within the study area

are confined to depths >~12 km along NE-dipping décollement faults that strike perpendicular to the convergence direction. In contrast, dextral strike–slip focal mechanisms are recorded at shallower depths under the trace of the MRF. This difference in the depth of the focal mechanisms suggests that the upper crust deforms mostly by slip on weak, pre-existing faults, either strike–slip or thrust, but that the lower crust is more homogeneous and accommodates shortening by reverse faulting perpendicular to the regional motion (Hatzfeld et al. 2010). Most of the earthquakes in the study area are compressional dip–slip and strike–slip, with epicenters at depths between ~10 and ~20 km (Figs. 7, 8).

Inversion of earthquake focal mechanism and fault–slip data

To reconstruct the paleo and recent stress states within the study area, we applied two methods: (1) inversion of the earthquake focal mechanisms and (2) inversion of fault–slip data.

To determine the present-day stress pattern in the western Fars, we used inversion of the earthquake focal mechanisms described by previous studies (McKenzie 1969; Otsubo et al. 2008; Yamaji et al. 2011). Fault–slip analyses and paleo-stress methods are commonly applied to infer different phases of extension and shortening (Angelier 1990; Zalohar and Vrabec 2007). We applied inversion of the slickenlines on fault planes (Mukherjee 2014, 2015b; Kaplay et al. 2017; Misra and Mukherjee 2017; Dasgupta and Mukherjee 2017) to constrain the stresses responsible for older phases of deformation. Both these methods are based on the Wallace–Bott hypothesis that expresses the slip vector of an earthquake as parallel to the resolved shear stress on the fault (Wallace 1951; Bott 1959).

Earthquake focal mechanism inversion method

The multiple inverse method (MIM) (Yamaji et al. 2011) is a numerical technique for determining the stress directions
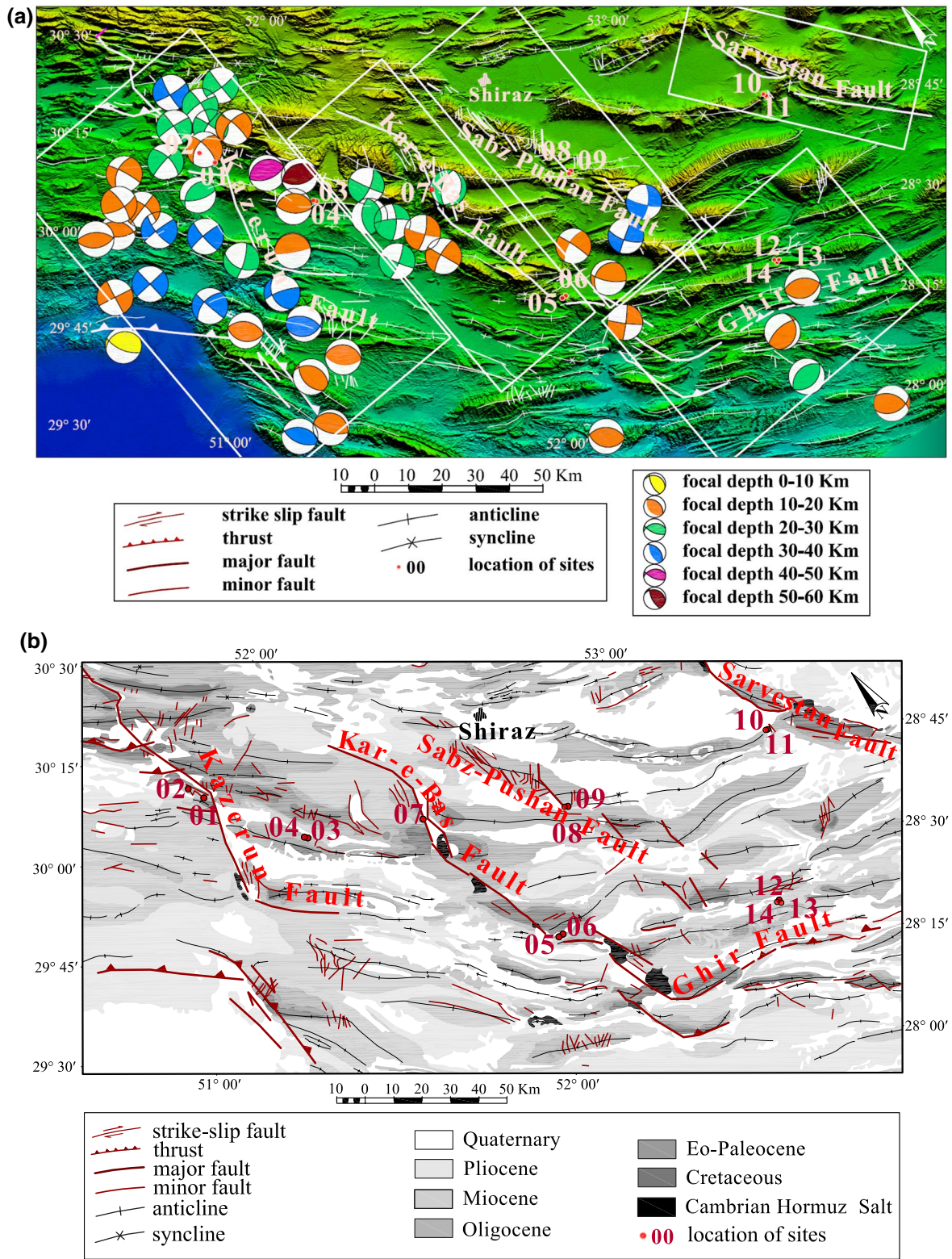
Fig. 8 SRTM-structural map of the study area (**a**). Geological map of the study area (**b**), modified from the geological map of south central Iran, N.I.O.C, 1977; major active faults of Iran (Hessami et al. 2003); and tectonic map of Iran (Stöcklin and Nabavi 1973). Earthquake focal mechanisms obtained from GCMT and ZUR-RMT catalogue for the period between 1976 and 2012. Most of mechanisms are thrust and strike–slip

from the earthquake focal mechanism data. This method does not require a fault plane from the two nodal planes (Yamaji 2000b; Otsubo et al. 2008; Yamaji et al. 2011), because it assumes that both the nodal planes acted as the fault planes. On Mohr diagrams (Fig. 9), normal and shear stresses are normalized with values of 0–1 and 0–0.5, respectively. The resulting principal stresses are represented as clusters of reduced stress tensors (Otsubo et al. 2006, 2008). A reduced stress tensor represents the stress tensors that have ordinary principal orientations and a Φ value. If the fault attitudes and magnitude and direction of the normal and shear stress are known, the MIM software can calculate the misfit angles between the observed and theoretical fault–slip directions (Fig. 9) and minimize the sum of the misfit angles (Otsubo et al. 2008).

The MIM method has been used throughout the study area to determine the state of stress using available focal mechanisms. Because of the heterogeneity of the focal mechanism data, the study area was subdivided into five domains, where the state of stress is nearly homogeneous (Fig. 8). The results of orientations of the maximum and minimum principal stresses could be shown as clusters of points on the unit sphere for all earthquake focal mechanisms (Fig. 10). The clusters are identified using the *k*-means clustering algorithm (Otsubo et al. 2006). The tangent-lineation diagrams (Fig. 11) show the theoretical slip directions for the state of stress and the computed slip directions derived from inversions of the earthquake focal mechanisms.

The focal mechanism catalogue contains events with a moment magnitude $M_w > 4.2$, as reported by the Global Centroid Moment Tensor (GCMT) and the Zurich Moment Tensors (ZUR_RMT), for the period between 1976 and 2012 (Table 1). The data include the focal location, earthquake date and time, depth and magnitude of the earthquakes, the strike and dip of the nodal planes, the rake of the hanging-wall's slip direction, the fault mechanism, and the centers that reported the earthquakes (Table 1).

The data set contains 58 focal mechanisms: compressional dip–slip (~50%), extensional dip–slip (~3%), oblique–slip (~9%), and strike–slip (~38%) mechanisms (Fig. 8). The study area is subdivided into five domains that include the five major fault zones (Kazerun, Kar-e-Bass, Sabz-Pushan, Sarvestan, and Ghir fault zones) (Fig. 8). In each fault zone, the focal mechanisms of the earthquakes have been extracted to reveal the present-day stress regime.

In the Zagros Foreland Folded Belt (F-FOB) and Zagros foreland fold-and-thrust belt (F-FATB), the earthquake locations are not sufficiently accurate to justify linking seismic events to specific faults or to obtain precise focal depths because of the sparse seismic network and absence of an accurate crustal velocity model. On the other hand, the accuracy of the earthquake locations is approximately

20 km (Engdahl et al. 1998; Hatzfeld et al. 2010). Based on this deficiency, we have allocated a wide area (~15′ or ~30 km wide) around each fault zone (Fig. 8).

To infer the present-day state of stress in the Fars salient, we applied the stress inversion method to the focal mechanism data. The data are the azimuth and dip of two nodal planes and the rake of the lineations. The stress inversion methods assume a uniform state of stress. To interpolate the *P*- and *T*-axes (approximations of maximum and minimum principal stress directions), the method yields the principal stress axes and ratio between the principal stress magnitudes. The misfit angle is the angle between the measured slickenlines and the calculated relative shear stress, τ. Following the MIM (Yamaji et al. 2011), the ellipsoid has axes that are parallel to the principal stress axes and radii *X*, *Y*, and *Z* (with $X \geq Y \geq Z$), satisfying the relation that $(Y–Z)/(X–Z)$ equals the Φ value of the stress state (Table 2). Shape ratio Φ has a value between 0 and 1; Φ = 0 for a prolate stress ellipsoid, where $\sigma_2 = \sigma_3$ (uniaxial compression); Φ = 1 implies that the stress ellipsoid is oblate and $\sigma_1 = \sigma_2$, (uniaxial tension) (Fossen 2016).

Fault–slip inversion method

Study of the paleo-stress field helps us for better understanding deformation of orogenic belts and the migration of hydrocarbon and/or hydrothermal fluids. The kinematics of a fault zone are defined using slickenlines that were produced by a few millimeters to several meters of movement along a fault plane. For each fault, the strike and dip of fault plane, the rake orientation of lineation, and the sense of movement were measured in the field and recorded (Fig. 12). These data are the results of many measurements over the large areas around each fault. To infer the stress state that is responsible for the deformation in the study area, we inverted distinct groups of slip data measured at individual sites using the Gauss method (T-Tecto software) of Zalohar and Vrabec (2007).

The fault–slip inversion method assumes that (1) the rock body is mechanically homogeneous and isotropic; (2) the rock has a linear viscous rheology (Twiss and Unruh 1998; Lacombe 2012); (3) displacements on the fault planes are small with respect to their lengths and there is no ductile deformation and, thus, no rotation of the fault planes; (4) a tectonic event is characterized by a single homogeneous stress tensor; (5) the fault plane is a pre-existing fracture and the slip responsible for the slickenlines occurs in the direction of maximum resolved shear stress; and (6) the slip on each fault plane is independent of the slip on all other fault planes. Some authors (e.g., Twiss and Unruh 1998) claim that because of the different orientations of the stresses inside and outside the fault zone, the linearity and isotropy behavior of the fault zone cannot be used as an assumption for inferring
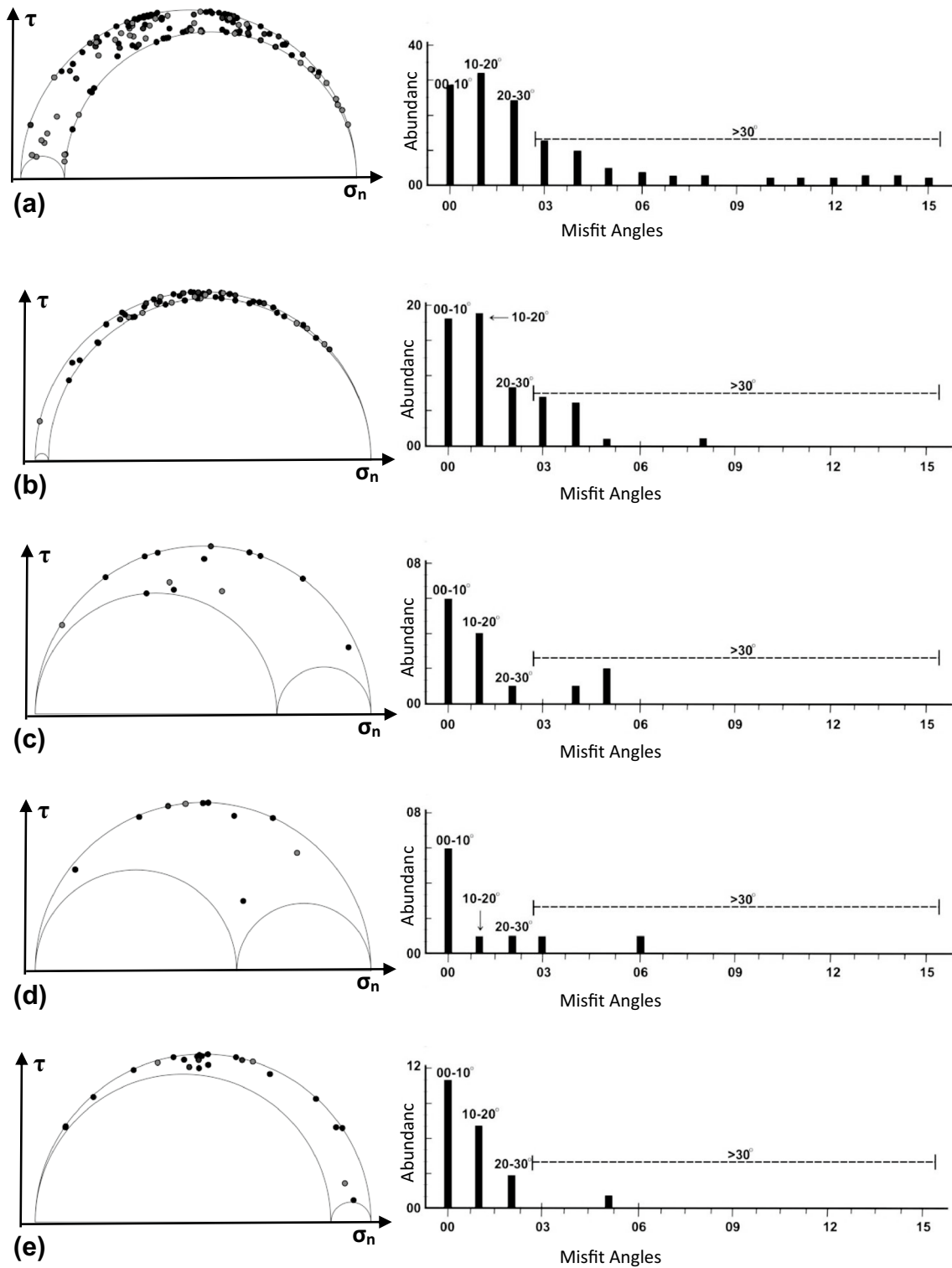
Fig. 9 3D Mohr diagrams (on the *left*) and misfit angle histograms (on the *right*) as derived from inversion of earthquake focal mechanisms. **a–e** All earthquakes in case study area, Kazerun fault, Kar-e-Bass fault, Sabz-Pushan fault, and Ghir fault, respectively. The normal and shear stresses on the faults are plotted on 3D Mohr diagrams
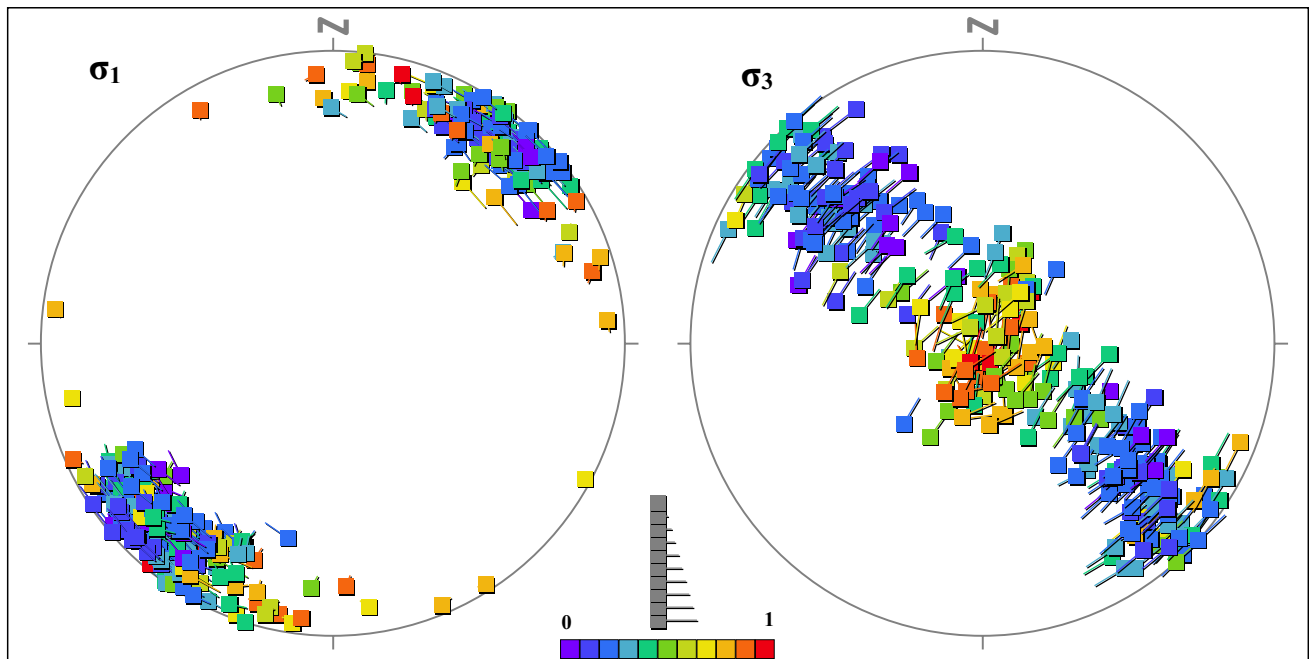
Fig. 10 Orientations of maximum and minimum principal stresses for all earthquakes in the study area, plotted on lower hemisphere, equal-area projections, resulting from multiple inverse method using the MIM software (Yamaji et al. 2011). Lengths of *bars* shown in the *lower middle* of the figure indicate the plunge of stress axes. At the *bottom* of the figure, the *color* of the *squares* is related to the Φ value

the stress from inversion of fault–slip data. They also mention that the degree of inaccuracy would depend on the degrees of anisotropy and non-linearity, which at present remain unknown. However, at the regional scale, the stress field can be analyzed in the region that be divided into smaller more homogeneous sub-domains which has much more isotropy and linearity. As a result, it is reasonable to compare results of inversion of fault–slip data with contemporary stresses (e.g., the stress derived from earthquake focal mechanisms), and try to combine both results to better understand the mechanical behavior of the continental crust (Lacombe 2012).

The basic principle involves finding the best fit between the observed directions and senses of slip on the numerous faults and theoretical shear stress on these planes. Similar to the inversion of the earthquake focal mechanisms, the results are reported as the trend and plunge of the three principal stress axes, σ_1, σ_2, and σ_3, and the ratio $\Phi = (\sigma_2 - \sigma_3)/(\sigma_1 - \sigma_3)$, which describes the shape of the stress ellipsoid, and thus, the nature of the stress regime (for example, if σ_3 is vertical and Φ close to 0, it indicates a reverse/strike–slip regime) (Bott's 1959; Fossen 2016). Numerical estimators, such as the average misfit angle between the computed shear stresses and the actual slickenlines on fault planes, record the validity of the calculated tensor. The absolute values of the stress components cannot be determined, but the optimal principal orientations and stress ratio are obtained using Gauss-inverse method. Unlike the results obtained from the inversion of the focal

mechanism, the results of the fault–slip data refer to deformation within the sedimentary cover.

If the observed tilted bedding is a result of folding, the faults in that region may have formed before, during, or after folding. In the case where faults formed before folding, the striations should be back rotated before analysis and interpretation (Lacombe et al. 2006). Anderson (1951) suggested that one of the three principal stress axes is generally vertical (or horizontal) in major fault zones, but the slight departures from this rule (<10°, that have been seen in some of our measurements) are common (McGarr and Gay 1978). If a fault was active before folding and was subsequently passively tilted with the bedding, the stress tensor calculated on these data does not have a vertical (or horizontal) axis. Instead, one of the stress axes is generally perpendicular to the bedding, whereas the two other stress axes are along the bedding plane. In these cases, the fault system should be analyzed after back tilting to its initial position (Lacombe et al. 2006). Accordingly, sites 9 and 10 within the Sarvestan fault zone and sites 11, 12, and 13 within the Ghir fault zone were back tilted before interpretation (Fig. 13).

Age estimation for fault–slip formations

Some authors (e.g., Angelier 1991; Yamaji et al. 2005; Lacombe et al. 2006; Navabpour et al. 2007; Sperner and Zweigel 2010) believe that the relative age of the
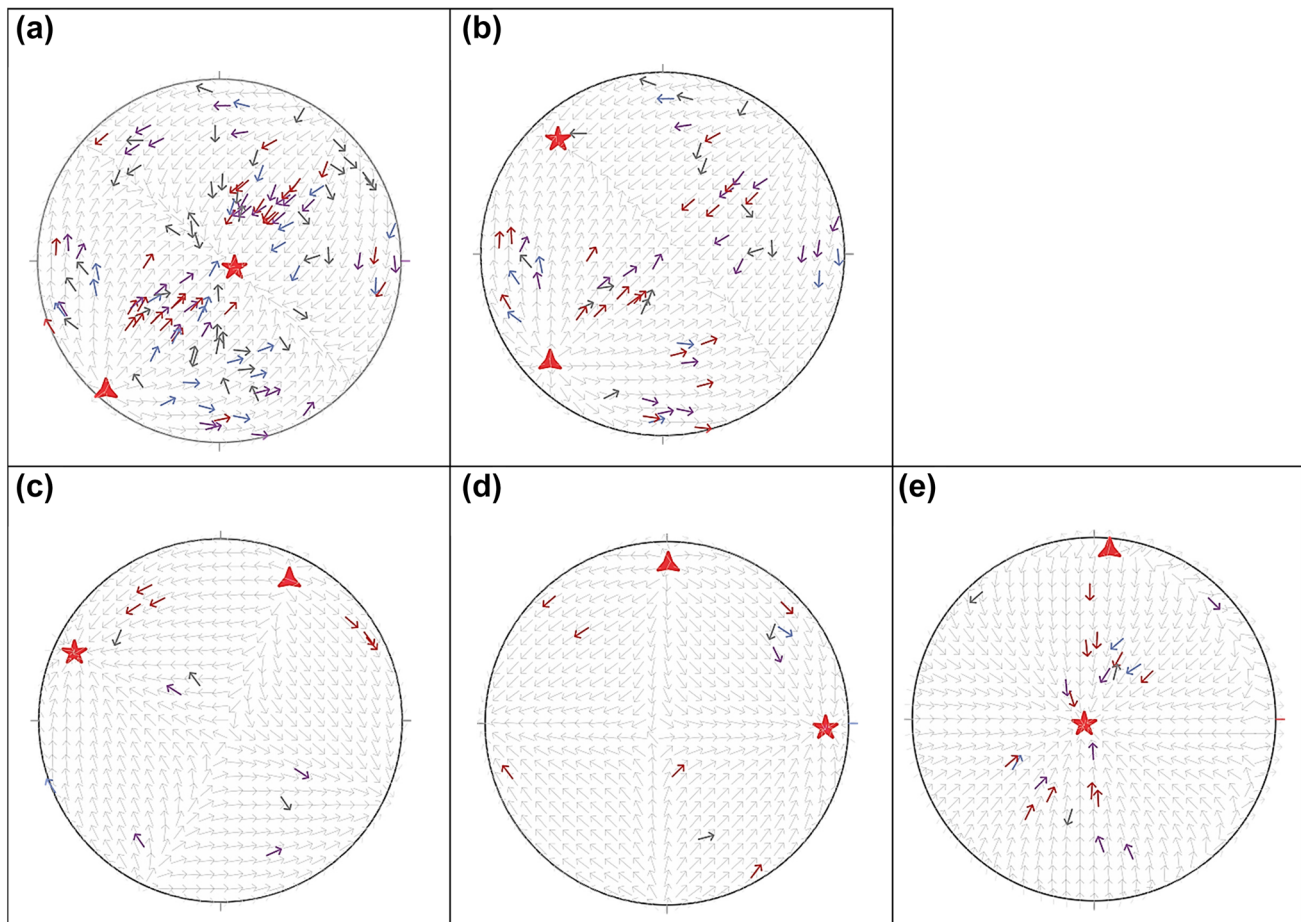
Fig. 11 Tangent-lineation diagrams derived from inversion of earthquake focal mechanisms and theoretical slip directions (*thin gray arrows*) for the state of stress (lower hemisphere, equal-angle projection). The slip on the fault planes is represented by *thick colored arrows* plotted on a stereonet. The position of the *arrows* in the diagram indicates the pole to the fault plane. The *symbols red triangles* and *red stars* denote the σ_1- and σ_3-axes, respectively. **a** All of the faults in the study area: **b** Kazerun fault zone, **c** Kar-e-Bass fault zone, **d** Sabz-Pushan fault zone, and **e** Ghir fault zone

fault–slip events can be estimated based on: (1) the recognized sequences of faulting and folding, the chronology of two superposed and differently oriented fiber lines on a fault plane; (2) the ages of deformed units of known stratigraphy; and (3) the horizontal axis rotations of the stratigraphy from folding. Furthermore, at locations with significant layer tilting, brittle events must be dated with reference to the folding. On other hand, some authors (e.g., Hippolyte et al. 2012) note that these methods of estimating the timing of fault–slip are often difficult to determine with confidence. The inversion of the fault–slip data results in a mean stress tensor that is averaged over time (several thousands or millions of years) and space (the volume of rock containing the analyzed faults), and without an exact dating method, the actual time of faulting cannot be well constrained. In our study, we do not have a way to determine the exact age of the slickenlines. However, we have assumed that the age of the

the slip events on the faults is confined between the depositional ages of the faulted rocks and the present. In the case where the striations formed before folding (within the Sarvestan and Ghir fault zones), the age of the slickenlines is interpreted as older than initial fold development. At other sites, the age of the stress state places the event after folding. In general, we know that the stress regimes obtained from the focal mechanism inversion are definitely younger than the stress regimes obtained from inversion of the fault–slip data.

Results of stress analyses

Earthquake focal mechanism inversion

Because earthquakes with higher magnitudes yield more accurate nodal plane locations and geometries (e.g.,

Table 1 Earthquake parameters used for stress determination

Lat	Lon	Date	Time	Depth	M_w	Az_1	D_1	S_1	Az_2	D_2	S_2	Mech.	Ref.
29.99	51.05	20110305	112444	12.0	5.3	126	41	93	302	49	87	T	GCMT
29.87	51.06	19880811	160008	15.0	5.8	283	69	7	190	84	159	SS	GCMT
29.96	51.11	19920911	120609	15.0	5.3	302	33	67	148	60	104	T	GCMT
29.76	51.12	19961118	115216	33.0	5.2	177	62	−177	85	87	−28	SS	GCMT
29.02	51.19	20020413	065823	15	4.4	326	54	78	166	37	106	T	ZUR_RMT
29.08	51.23	19940329	075659	33.0	5.1	334	40	104	136	52	79	T	GCMT
29.57	51.23	20020601	161239	33.0	5.0	261	58	2	170	88	148	OS	GCMT
29.99	51.23	20010523	023113	12	4.6	4	75	160	99	71	16	SS	ZUR_RMT
29.93	51.25	20000623	061512	33.0	5.1	180	75	175	272	85	15	SS	GCMT
29.97	51.25	19861220	234709	15.0	5.4	348	70	−179	257	89	−20	SS	GCMT
30.07	51.26	19880830	173020	15.0	5.1	242	57	−9	337	83	−147	OS	GCMT
29.45	51.29	20020909	075651	15	4.4	318	50	90	139	40	91	T	ZUR_RMT
29.05	51.31	19901216	221856	15.0	5.7	332	23	97	144	67	87	T	GCMT
29.79	51.36	19860712	075431	33.0	5.7	178	81	172	269	82	10	SS	GCMT
29.20	51.39	20010506	053928	18	4.3	178	54	107	330	40	68	T	ZUR_RMT
29.64	51.42	19890503	091320	29.6	5.2	153	55	−166	55	78	−36	OS	GCMT
29.20	51.44	20000313	111619	15.0	4.6	135	56	89	316	34	91	T	ZUR_RMT
30.02	51.46	20101201	195544	23.4	4.9	355	68	−172	262	82	−22	SS	GCMT
29.88	51.47	20040508	043925	21	4.5	113	70	52	360	43	149	T	ZUR_RMT
29.36	51.48	19991031	150944	33.0	5.2	117	34	67	324	58	105	T	GCMT
29.45	51.50	20030527	103056	33.0	5.3	189	46	165	290	79	45	OS	GCMT
30.08	51.56	20110105	055547	21.3	5.4	5	84	−174	274	84	−6	SS	GCMT
30.00	51.58	19881206	132046	15.0	5.9	256	54	−20	357	74	−142	OS	GCMT
30.18	51.60	20020829	095349	33	4.6	98	82	−9	189	82	−172	SS	ZUR_RMT
29.56	51.62	20100927	112248	17.1	5.9	309	6	100	119	85	89	T	GCMT
30.10	51.62	20110108	002426	20.5	5.1	275	78	−11	7	80	−168	SS	GCMT
30.03	51.64	20110107	235303	23.6	5.0	252	74	−6	343	84	−164	SS	GCMT
30.00	51.69	19880811	160449	15.0	6.0	256	63	−12	351	79	−152	SS	GCMT
29.67	51.71	20020516	110012	18	4.4	135	61	98	298	30	75	T	ZUR_RMT
29.80	51.71	20031003	123450	45	4.7	109	62	91	287	28	88	T	GCMT
30.12	51.72	20000706	083429	24.0	4.7	181	88	−171	91	81	−2	SS	ZUR_RMT
29.71	51.73	20031004	124434	51	4.6	115	56	93	289	34	86	T	GCMT
29.37	51.92	20020603	013527	24.0	4.4	151	86	−170	60	80	−4	SS	ZUR_RMT
29.52	51.94	20031003	021408	18	4.9	213	56	−90	33	34	−90	T	GCMT
29.59	51.96	20020517	035220	24	4.9	153	86	−163	62	73	−4	SS	ZUR_RMT
29.46	51.97	20010424	081309	27	4.3	304	77	162	39	72	14	SS	ZUR_RMT
29.31	52.02	19930106	225146	15.0	5.4	248	76	0	339	90	−166	SS	GCMT
29.34	52.03	19990506	230058	17.4	6.2	52	76	−6	143	84	−165	SS	GCMT
28.49	52.08	19760422	170310	15.0	5.6	141	41	98	310	49	83	T	GCMT
29.45	52.19	20010609	044533	24	4.6	232	60	−93	58	30	−85	N	ZUR_RMT
27.98	52.30	19930329	152044	40.0	5.2	104	28	72	305	64	99	T	GCMT
28.75	52.42	19940301	034904	17.0	6.0	136	85	−176	46	86	−5	SS	GCMT
29.06	52.44	19940620	090906	15.0	5.9	251	67	−5	343	85	−157	SS	GCMT
27.94	52.47	20101126	123346	12.0	5.5	281	42	70	128	51	107	T	GCMT
28.90	52.52	20050809	050923	16.1	5.1	257	30	31	139	75	117	T	GCMT
28.96	52.60	19940330	195543	33.0	5.4	148	71	177	239	87	19	SS	GCMT
29.01	52.72	19940403	065158	33.0	5.2	47	69	−11	142	79	−159	SS	GCMT
28.26	52.83	20021006	095145	24.0	4.5	267	47	92	84	43	88	T	ZUR_RMT
28.40	52.85	20000301	200632	15.0	5.0	49	26	55	267	69	106	T	GCMT
27.90	53.00	19860503	103743	15.0	5.2	111	33	60	325	62	108	T	GCMT
28.03	53.02	19860502	031840	15.0	5.5	107	47	57	331	52	121	T	GCMT

Table 1 (continued)

Lat	Lon	Date	Time	Depth	M_w	Az_1	D_1	S_1	Az_2	D_2	S_2	Mech.	Ref.
28.48	53.03	20030316	054204	18	4.3	300	51	96	112	39	83	T	ZUR_RMT
28.22	53.48	19850202	205234	21.6	5.4	114	32	−81	284	58	−95	N	GCMT
28.19	53.66	20031128	231952	33.0	5.0	43	19	60	255	74	100	T	GCMT
27.95	53.85	19830218	074026	15.0	5.2	272	20	94	88	70	89	T	GCMT
28.39	53.86	20031215	225727	15.0	5.1	272	43	90	92	47	90	T	GCMT
28.34	53.91	20031024	055824	33.0	5.0	128	39	70	333	54	105	T	GCMT
29.66	50.80	20000305	090100	5.0	5.1	292	26	53	152	69	6	T	ZUR_RMT

Az1 Azimuth of nodal plane 1, *D1* dip of nodal plane 1, *S1* rake of slip in the nodal plane 1, *Az2* Azimuth of nodal plane 2, *D2* dip of nodal plane 2, *S2* rake of slip in the nodal plane 2, *Mech.* mechanism of faulting, *T* thrust faulting, *N* normal faulting, *SS* strike–slip and *OS* oblique–slip faulting, *Ref.* the references that data have been obtained, *GCMT* global centroid moment tensor, *ZUR_RMT* Zurich moment tensors

Table 2 Results of inversion of the earthquake focal mechanisms

Location	$T\sigma_1$	$P\sigma_1$	$T\sigma_3$	$P\sigma_3$	Φ
Kazerun fault	S46°W	09°	N42°W	09°	0.04
Kar-e-Bass fault	N26°E	08°	N65°W	08°	0.72
Sabz-Pushan fault	N00°E	08°	S88°E	08°	0.6
Ghir fault	N05°E	04°	S63°W	83°	0.88

$T\sigma_1$ and $P\sigma_1$ indicate trend and plunge of maximum compression, and $T\sigma_3$ and $P\sigma_3$ represent trend and plunge of minimum compression. Φ is the shape ratio (see Fig. 14)

Hatzfeld 1999; Maggi et al. 2002), we have used earthquakes with moment magnitudes $M_w \geq 4.2$ in our analysis. Most of the thrust earthquakes (between 1968 and 2000, Talebian and Jackson 2004) occur along the SW Zagros margin, between the coastal plain of the Persian Gulf and the Surmeh–Ghir thrust system, while the strike–slip earthquakes are closely associated with the Kar-e-Bass and Sabz-Pushan fault zones (Fig. 6; Lacombe et al. 2006). The Kazerun fault zone has both compressional dip–slip and strike–slip motions, and the Ghir fault zone is dominantly compressional dip–slip (Fig. 8).

Because the seismicity in the central Zagros is beneath the sedimentary cover and in the upper part of the basement (Tatar et al. 2004; Hatzfeld et al. 2010), the results obtained from inversion of the focal mechanism refer to the foreland gneissic basement.

Kazerun fault zone

Among the 58 earthquakes focal mechanisms (recorded from 1976 to 2012), 33 occurred within the Kazerun fault zone (latitude 29°–30.5°; longitude 51°–52°, Table 1).

For the Kazerun fault, the trend and plunge of σ_1 and σ_3 are S46°W′09° and N42°W′09°, respectively, and the stress ratio $\Phi = 0.04$. These results indicate a strike–slip faulting regime with NE–SW compression and NW–SE tension (Table 2; Fig. 14).

Kar-e-Bass fault zone

Seven focal mechanisms from the earthquakes (latitude 28.5°–29.5°; longitude 52°–52.5°) within the Kar-e-Bass fault were analyzed.

For the Kar-e-Bass fault zone, the trend and plunge of σ_1 and σ_3 are N26°E′08° and N65°W′08°, respectively, and the stress ratio is $\Phi = 0.72$. These results also indicate a strike–slip faulting regime with NE–SW compression and NW–SE tension (Table 2; Fig. 14).

Sabz-Pushan fault zone

Five focal mechanisms from earthquakes with latitudes between 28.5° and 29.5° and longitudes between 52.5° and 53° within the Sabz-Pushan fault zone reveal the orientations of σ_1 and σ_3 to be N00°E′08° and S88°E′08°, respectively, and that the stress ratio Φ is equal to 0.6. These results indicate a strike–slip faulting regime with N–S compression and E–W tension (Table 2; Fig. 14).

Ghir fault zone

An analysis of 13 focal mechanisms from earthquakes with latitudes between 28.5° and 29.5° and longitudes between 52° and 52.5° within the Ghir fault zone reveal the σ_1 and σ_3 orientations to be N05°E′04° and S63°W′83°, respectively, and the stress ratio to be 0.88. This solution indicates a thrust faulting regime with N–S compression and NE–SW tension (Table 2; Fig. 14).

Fault–slip inversion

To evaluate the paleo-stress regime of the Kazerun, Kar-e-Bass, Sabz-Pushan, Sarvestan, and Ghir fault zones, we defined suitable sites along each fault and measured the strike and dip of the fault plane, rake of the slickenline, and polarity of movement for each one in the field. For more accuracy, all measurements have been done with
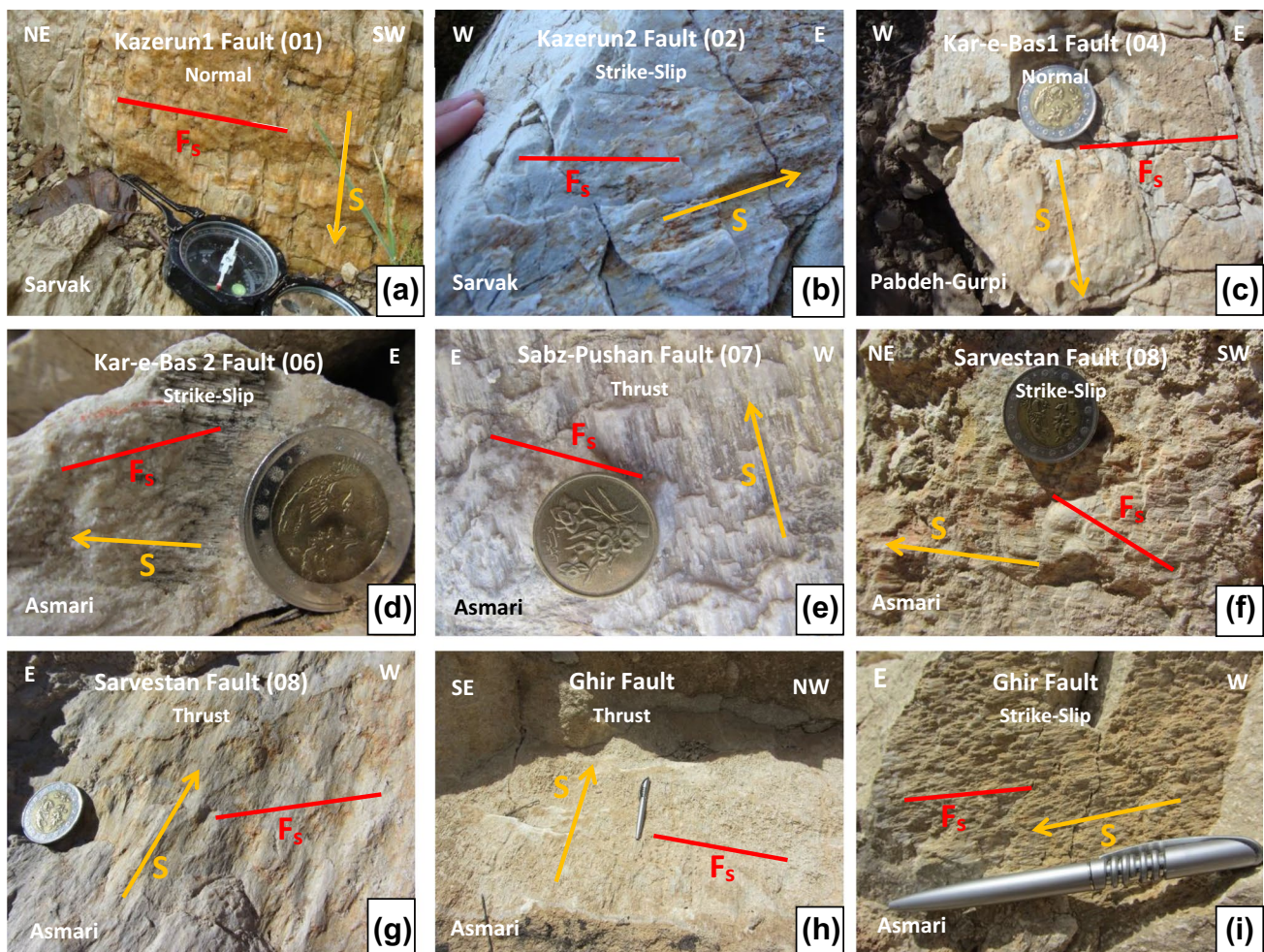
Fig. 12 Representative sample field images of the fault planes. The types of kinematic indicators are TM1 and TM2 of classification of Doblas ([1998](#)). Slickenlines and strike of fault planes are indicated with S and F_S, respectively. The sense of movement is presented by the *yellow arrows*. The formations are Asmari limestone, Pabdeh marly shale, and the Sarvak limestone. The length of coin diameter is 2.7 cm

Brunton compass. In each fault zone, the number of sites and measurements is shown in Table 3. According to field observations and Anderson ([1951](#)), the fault systems in sites 10 and 11 in the Sarvestan fault zone and sites 12, 13, and 14 in the Ghir fault zone were back tilted prior to interpretation and analysis (Fig. [13](#); Table [3](#)). The attitude (strike and dip) of the tilted beds belong to Sarvestan and Ghir faults are S70°W′30°NW and S75°E′30°SW, respectively. For back tilting, the tilted layer was rotated on equal-area or equal-angle stereonets to be horizontal; the related faults were rotated as the same angle and direction.

Varied stress regimes are specified by different orientations of the principal stress axes. The inversion of the fault–slip data for the study area revealed stress regimes varying from compressional to tensional dip–slip and

strike–slip for the Kazerun, Kar-e-Bass, Sabz-Pushan, Sarvestan, and Ghir fault zones. Table [3](#) and Figs. [15](#), [16](#) show the results of the analysis for each fault zone in the study area. As shown in Fig. [15](#), most sites have NE–SW compression, consistent with the convergence between the Afro–Arabian and Eurasian continent. The middle segment of the Kar-e-Bass fault zone (site 07) indicates the compressional trends ~130° and is incompatible with the compression direction measured in other fault zones. All the data have been measured from three major formations that have different ages. The compressional trend is slightly different in different formations (Tables [3](#), [4](#)). Although the time of sedimentation has been known, without an exact dating method, the actual time of faulting cannot be well constrained (see "[Age estimation for fault–slip formations](#)").
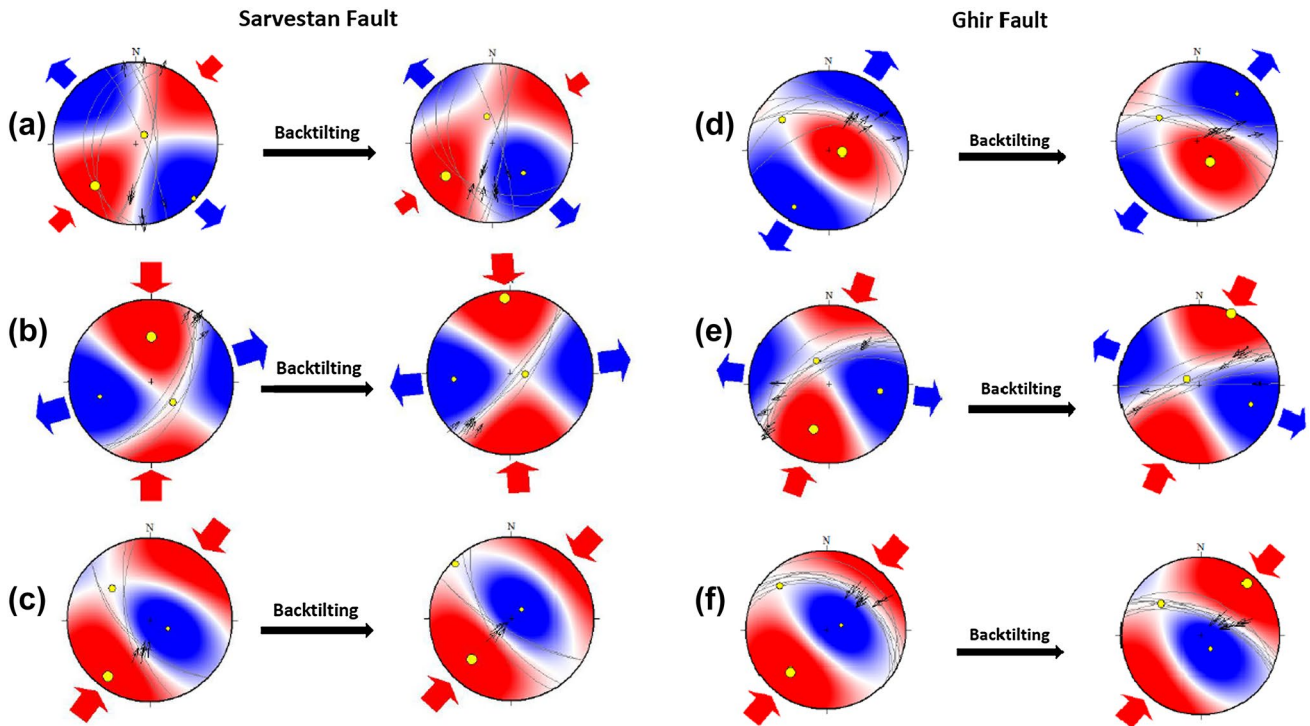
Fig. 13 Results of fault–slip inversion within the Sarvestan fault (in the *left*) and Ghir fault (in the *right*) before and after tilting. **a–c** Dextral, sinistral, and reverse mechanisms of Sarvestan fault, and **d–f** normal, strike–slip, and reverse mechanisms of Ghir fault, respectively. The attitude (strike and dip) of the tilted bed belong to Sarvestan and Ghir fault is 070°/30°NW and 285°/30°SW, respectively

Fig. 14 Geological map of the study area showing maximum and minimum principal stress orientations based on inversion of earthquake focal mechanism data for each fault zone (see Table 2)
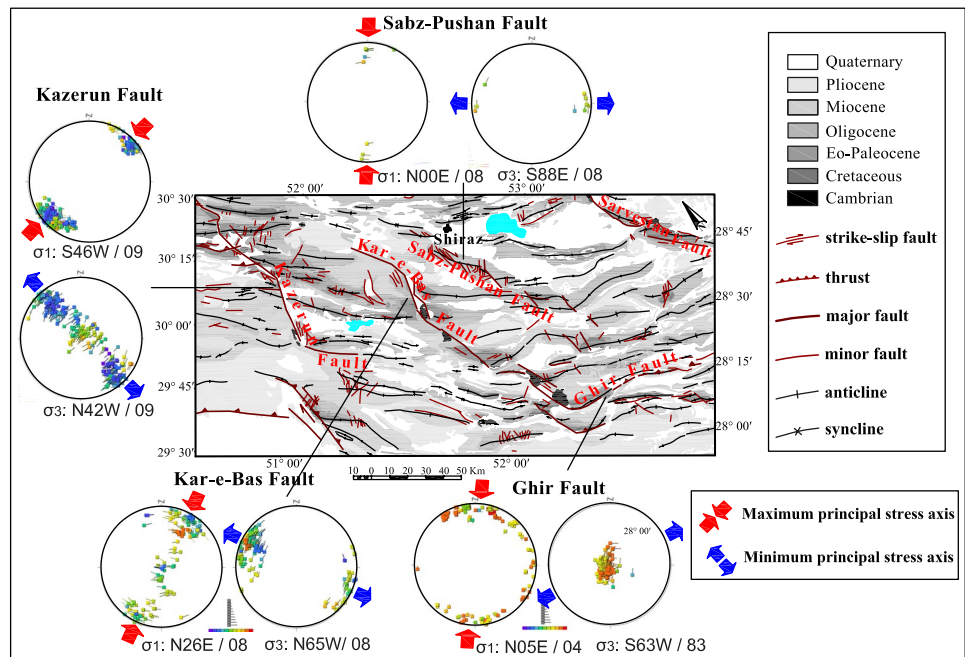
Discussion

The stress regimes obtained by inverting the fault–slip data may be local or regional. Only results that are consistent throughout the entire area can be considered tectonic regimes (Lacombe et al. 2006). Thus, the results obtained from the sites with a small spread of slickenlines have been eliminated. In each fault zone (Kazerun, Kar-e-Bass,
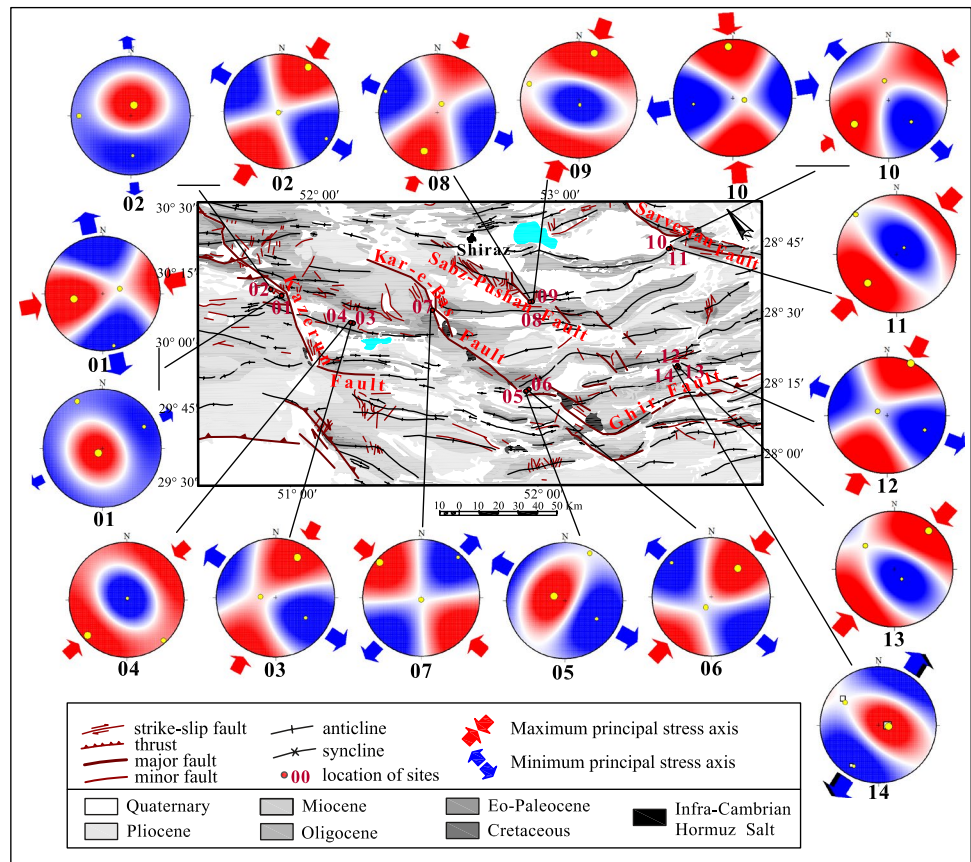
Table 3 Results of inversion of fault–slip data

Site no.	Site	Latitude	Longitude	Formation	Number of data	$T\sigma 1$	$P\sigma 1$	$T\sigma 2$	$P\sigma 2$	$T\sigma 3$	$P\sigma 3$	Φ	α
01	Kazerun1, normal fault	29°56′16″	51°35′10″	Sarvak	9	220	78	332	05	063	12	0.1	14
01	Kazerun1, strike–slip fault	29°56′16″	51°35′10″	Sarvak	9	260	35	074	55	168	03	0.5	7
02	Kazerun2, normal fault	29°58′40″	51°34′19″	Sarvak	5	017	69	270	06	177	20	0.3	3
02	Kazerun2, strike–slip fault	29°58′40″	51°34′19″	Sarvak	18	031	05	250	84	121	04	0.5	16
03	Tang-e-Abulhayat, strike–slip fault	29°38′33″	51°47′23″	Asmari	16	031	13	273	64	124	22	0.2	14
04	Tang-e-Abulhayat, thrust fault	29°38′15″	51°47′30″	Asmari	7	228	04	138	01	027	87	0.6	10
05	Kar-e-Bass1, normal fault	28°54′55″	52°16′22″	Pabdeh	8	291	67	028	03	119	24	0.3	7
06	Kar-e-Bass1, strike–slip fault	28°54′32″	52°17′13″	Asmari	7	043	22	207	67	311	06	0.2	7
07	Kar-e-Bass2 fault	29°27′16″	52°09′26″	Asmari	23	311	02	197	86	041	04	0.3	17
08	Sabz-Pushan, strike–slip fault	29°12′13″	52°35′49″	Asmari	9	199	19	026	71	292	01	0.4	14
09	Sabz-Pushan, thrust fault	29°12′15″	52°35′47″	Asmari	40	018	08	288	05	167	80	0.8	7
10	Sarvestan, sinstral fault[a]	29°00′46″	53°19′21″	Asmari	5	355	06	101	67	261	21	0.1	3
10	Sarvestan, dextral fault[a]	29°00′46″	53°19′21″	Asmari	10	233	27	001	50	129	27	0.3	8
11	Sarvestan, thrust fault[a]	29°00′46″	53°19′22″	Asmari	5	224	20	315	02	050	71	0.5	2
12	Ghir, strike–slip fault[a]	28°34′17″	52°58′55″	Asmari	16	024	00	293	70	112	20	0.2	13
13	Ghir, thrust fault[a]	28°34′18″	52°58′54″	Asmari	8	042	06	309	24	145	65	0.2	5
14	Ghir, normal fault[a]	28°34′17″	52°58′54″	Asmari	7	152	56	300	29	039	16	0.3	13

$T\sigma 1$, $P\sigma 1$, $T\sigma 2$, $P\sigma 2$, $T\sigma 3$, and $P\sigma 3$ represent the trend and plunge of the principal stresses ($\sigma 1$, $\sigma 2$, and $\sigma 3$, respectively). Φ is the shape ratio and α is the misfit angle

[a] The sites were back tilted before interpretation (see Figs. 13, 15)

Fig. 15 Stress orientations from inversion of fault–slip data. Site numbers are listed below the spheres (see Table 3)

Fig. 16 Stress ellipsoids showing the proportions of σ_1 (*red line*), σ_2 (*green line*), and σ_3 (*blue line*) axes and their orientations calculated from inversion of fault–slip data. Φ (shape ratio) is listed near each ellipsoid
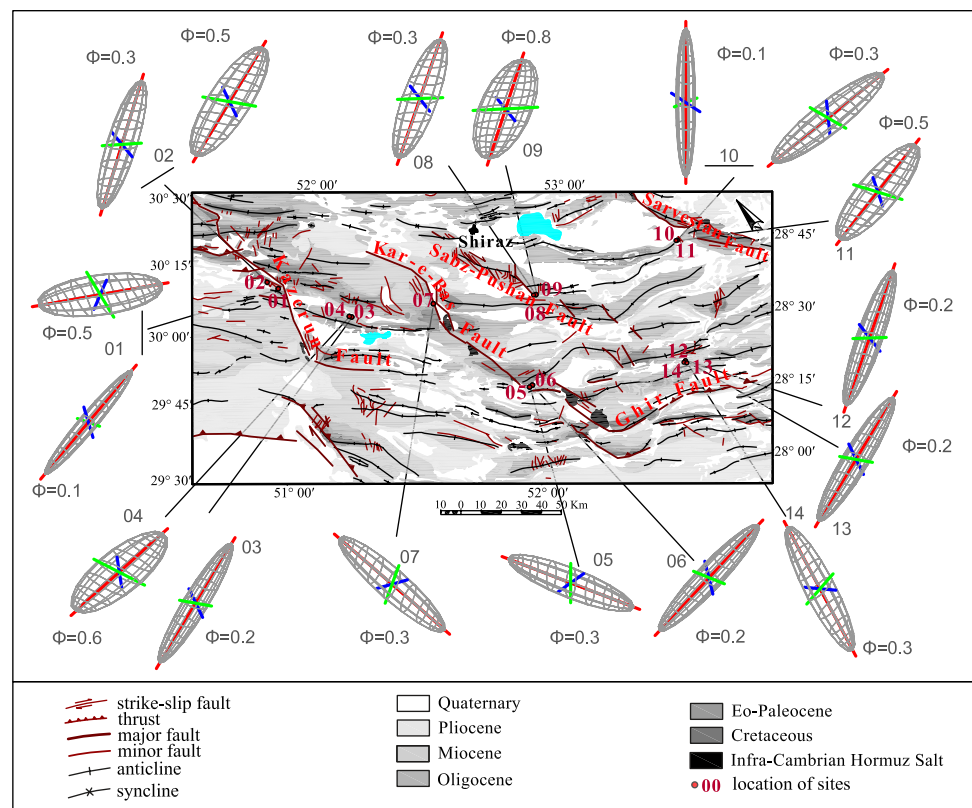
Table 4 Overview to paleo-stress chronostratigraphy

Formation	TU	No.	CD	FR
Asmari	Oligocene	12	NNE–SW	Thrust, strike–slip faulting
Pabdeh–Gurpi	Paleocene–Eocene	1	NW–SE	Normal faulting
Sarvak	Upper Cretaceous	4	NE–SW	Strike–slip, normal faulting

Different formations that have different times of sedimentation indicate semi-different compressional trend

TU the time unit of sedimentation, *No* number of sites, *CD* the compressional direction, *FR* faulting regimes

Sabz-Pushan, Sarvestan, and Ghir fault zones), the inversion of both the earthquake focal mechanisms and fault–slip data provides information regarding the temporal and spatial changes in the tectonic stress regime in the study area (Tables 2, 3). These results allow us to illustrate changes in the direction of the principal compressional stress from the older deformation to the most recent deformation (Figs. 14, 15). The inversion of the earthquake focal mechanisms shows that the present-day compressional direction averages ~N19°E and is compatible with the general direction of the recent convergence between the Afro–Arabian and Eurasian continents (~N13°E at the longitude of 52°E, Vernant et al. 2004). From NW to SE (from Kazerun to Ghir fault zone), the spatial variation in the recent compressional trend has a counterclockwise rotation. This rotation is consistent with the spatial change of the Afro–Arabian–Eurasian convergence paths along the Zagros orogenic belt that

has been previously suggested (e.g., Vernant et al. 2004; Walpersdorf et al. 2006).

On the other hand, the fault–slip data produce an average trend of ~N38°E for the paleo-compression direction. These results are consistent with the results of stereographic projection of the folds within the study area (Fig. 17). The major fold axial planes are good kinematic indicators to estimate the compressional trend (Ramsay and Huber 1987; Doblas 1998).

The relative consistency of the results from the inversion of the focal mechanisms and the fault–slip data also suggests that there is not a significant temporal variation in the direction of compression from Tertiary to recent time in the study area, although there is an anticlockwise rotation of the compression through time (over ~56 Ma, Fig. 1). Fault–slip date inversion also shows an anticlockwise change of the compression from upper Cretaceous

Fig. 17 Structural map of the Fars area showing equal area, lower hemisphere stereographic projection of the folds. *Red capital letter* with number that is presented for each fold in the map has been written at the *bottom* of the stereonet
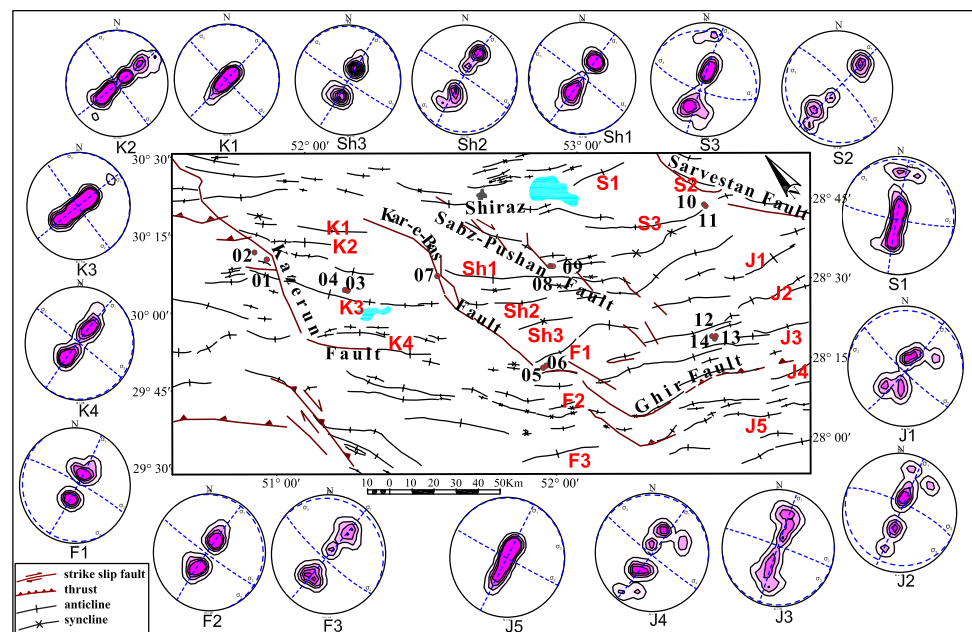
to Oligocene (Table 4). In upper Cretaceous, the compressional direction is NE–SW, while in Oligocene, it has rotated towards N. Although without the exact dating method, the actual time of faulting cannot be well constrained.

Inversion according to reconstructions of the long-term Afro–Arabian–Eurasian convergence paths (McQuarrie et al. 2003), the relative plate motion changed from N30°E (56–33 Ma) to N25°E (33–19 Ma), N09°E (19–10 Ma), and N05°E (last 10 Ma) (Fig. 1). Navabpour et al. (2007) used these results to suggest that the change in the convergence path over time presumably caused the change in the compressional directions. However, Lacombe et al. (2006) assert that the temporal change in the compressional trend obtained from tectonic analyses cannot be related to a change in plate kinematics over such a relatively short time span. They believe that it is more likely to reflect the local structural evolution of the Zagros orogenic belt within the framework of the Afro–Arabian–Eurasian continental convergence. We suggest that the variation in the compressional trend over time resulted from changes in the continental convergence path, but that it was also influenced by the local structural evolution, such as lateral propagation folds and the presence of several décollement horizons that allowed decoupling of deformation between the basement and the sedimentary cover (Oveisi et al. 2007).

Because the results that we have obtained from the inversion of the earthquake focal mechanism and the fault–slip data are from the foreland gneissic basement and sedimentary cover, respectively, the relative consistency between the results suggests that the compression has little inhomogeneity in both the overburden and the basement.

Consequently, there are few changes in the compressional trend between the upper crust and the ductile Hormuz salt décollement horizon. A comparison between the GPS surface displacement (Vernant et al. 2004; Tavakoli et al. 2008) with the early Pliocene compression in the Fars area (~5 Ma) supports this suggestion.

The lateral ramps and segmented strike–slip/dip–slip fault zones

Unlike the locations of the studies by Lacombe et al. (2006) and Navabpour et al. (2007), the locations chosen in our study were close to fault zones. The compatibility of our results with those of Lacombe et al. (2006) and Navabpour et al. (2007) (Fig. 18) indicates that, in the vicinity of the main lateral fault zones, the stress regime is similar to that in other parts of the Zagros orogenic belt. On the other hand, three lateral fault zones (Kar-e-Bass, Sabz-Pushan, and Sarvestan fault zones) as well as the Ghir thrust fault on both sides indicate an NNE–SSW compressional trend (the Kazerun fault indicates NE–SW compressional direction). The lateral faults are characterized by structures oblique to the belt. As Cotton and Koyi (2000) suggested from the results of sandbox modeling experiments, the development of transverse structures in response to a lateral change in the overburden thickness due to the basement geometry or a basin boundary or to the lateral termination of the main décollement horizon may occur in a thrust sheet moving over a décollement level. The consistency between the compressional trend of the Kar-e-Bass, Sabz-Pushan, and Sarvestan fault zones on both sides (previous studies, such as those of Lacombe et al. 2006; Navabpour

Fig. 18 Paleo-stress directions determined in this study compared with results of Lacombe et al. (2006) and Navabpour et al. (2007), showing high consistency
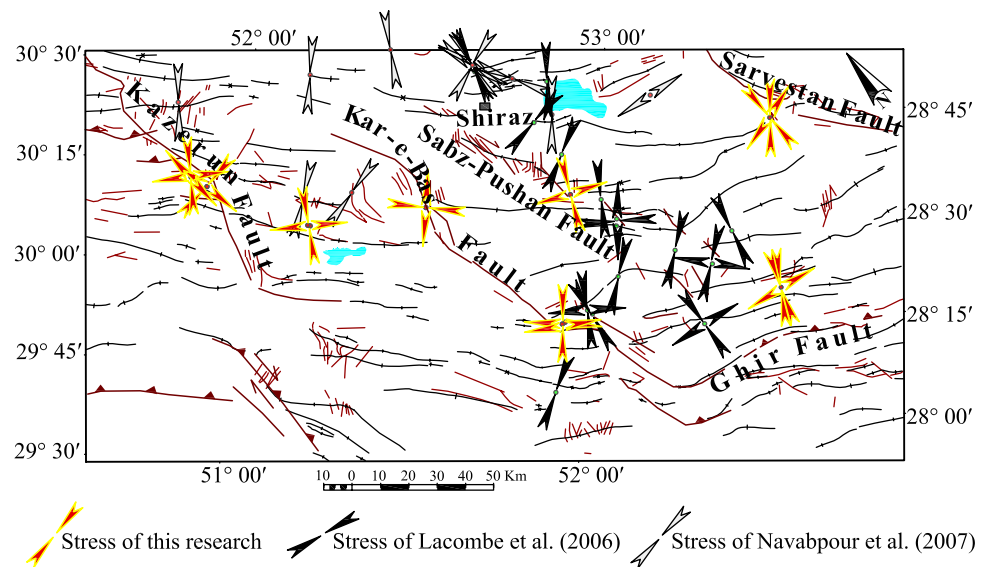
et al. 2007) and also the homogeneity of structural style of deformation on both sides of them, indicates that these fault zones may have initiated as primary tear faults in the sedimentary cover above the décollement horizon that formed in response to a lateral change in the cover thicknesses due to half graben inversion of the foreland gneissic basement. The temporal change in the compressional trend from NE–SW to NNE–SSW and/or block rotations is caused by change in behavior of the Kar-e-Bass, Sabz-Pushan, and Sarvestan fault zones from tear faulting to strike–slip faulting. This change could be coeval with the onset of the main phase of basement-involved shortening (Lacombe et al. 2006). The strike–slip and dip–slip-type basement earthquake events along the Kar-e-Bass, Sabz-Pushan, and Sarvestan fault zones and the related apparent lateral off-sets of folds in both basement and sedimentary cover (Berberian 1995; Lacombe et al. 2006) suggest that in recent times, these fault zones acted as segmented strike–slip and dip–slip faults in both the basement and the sedimentary cover. The obliquity of the maximum compressional stress into the fault trends reveals a typical stress partitioning of strike–slip and thrust motions in the Kar-e-Bass, Sabz-Pushan, and Sarvestan fault zones. The field evidences and seismic data support this suggestion that the Kar-e-Bass (Sarkarinejad and Zafarmand 2017b), Sabz-Pushan, and Sarvestan fault zones behave as segmented strike–slip and dip–slip faults.

Deep-seated earthquakes in vicinity of the Kazerun fault (Fig. 8), together with differences about 20°–30° in compressional trend between the Kazerun fault and other fault zones and also different structural style on both sides of Kazerun fault zone (Fars salient and Dezful embayment), show that Kazerun fault is a basement fault that it is infrastructure probably be different with other lateral fault

zones within the study area (Kar-e-Bass, Sabz-Pushan, and Sarvestan). Some authors (e.g., Sepehr and Cosgrove 2005; Burberry et al. 2011) suggested that Kazerun fault is one of the pre-collisional fault in the Zagros orogenic belt that was initiated in the Early Paleozoic as the extensional faulting. Therefore, we suggest that during early stages of continental collision, a gentle NW–SE trending within the Kazerun fault was initiated, and afterwards, this fault was reactivated as the segmented strike–slip and dip–slip fault. These reactivated segmented faults related to the asymmetrical half grabens are shown as double arrows in the crustal-scale Zagros orogenic belt (Fig. 4). Just like the other lateral faults (Kar-e-Bass, Sabz-Pushan, and Sarvestan fault zones), in the Kazerun fault zone, the obliquity of the maximum principal stress to the fault trend caused typical stress partitioning of dip–slip and strike–slip motion that led the Kazerun fault behaves as segmented dip–slip and strike–slip fault. The activities of the Zagros orogenic belt during transmission of collision-related compressional stress (Coward 1983; Ziegler et al. 2002) into the foreland strongly related either to the deep-seated basement inverted faults underlies the sedimentary cover or gently dipping shallow-seated décollement horizon of the rheological weak rocks of the infra-Cambrian Hormuz salt.

Recent-aseismic Sarvestan fault zone

Field evidence of the slickenlines on the fault planes suggests that the faults in the study area were active before quaternary (Tables 3, 4) and that there has not been a significant change during the quaternary. However, in recent times, the number of earthquakes decreases from the Kazerun to the Sarvestan fault zones, with no seismic activity on the Sarvestan fault (Fig. 8; Berberian 1995 suggested that no direct seismic

evidence has been found along the Sarvestan fault). Allen et al. (2013) suggested that the seismicity of the Zagros orogenic belt is influenced by the changes in elevation. Because the Kazerun, Kar-e-Bass, Sabz-Pushan, and Sarvestan fault zones are in the same structural zone (F-FOB) of the Zagros orogenic belt and there is not a large elevation difference between them, the effect of elevation on the reduction in seismicity along the Kazerun to Sarvestan faults is invalid. Two possible scenarios may explain the seismicity reduction between the Kazerun to Sarvestan fault zones: (1) tectonic shear stress variations from the Kazerun to Sarvestan fault zones and (2) locking along the Sarvestan fault. In support of 1, it seems that, presently, horizontal stress partitioning occurs, resulting in a higher resolved shear stress on the Kazerun and Kar-e-Bass faults, but less on the Sarvestan fault. In scenario 2, the Sarvestan fault may be currently locked due to the fault geometry or high friction; if so, there are consequences for seismic hazard assessments.

The NW–SE compressional regime

In the middle segment of the Kar-e-Bass fault zone (site 7), the NW–SE direction of compression is significantly different from the compression direction at the other sites. Lacombe et al. (2006) and Navabpour et al. (2007) also reported this inconsistency between different locations (especially between the Kar-e-Bass and Sabz-Pushan fault zones). In our opinion, three probable scenarios are reasonable. First, the sites that have a compression direction of approximately 130° are in the vicinity of salt diapirs, and the rheological contrast between the salt and the sediment may have affected the local stress distribution. Second, as per Berberian (1995), this site is located on a part of the Kar-e-Bass fault that bends and acts as a transfer fault, and the dextral sense of shear on the fault may create a trans-tension zone. Third, a northwest compressional event might have occurred in the Pliocene after the main phase of folding in the Zagros orogenic belt. However, as noted by some authors (e.g., Navabpour et al. 2007), the NW event is not reliably constrained relative to the other events. We suppose that the NW event is a real and significant event that occurred after folding. If so, the idea of anticlockwise rotation of the compressional trend through time is invalid.

Conclusions

- The compressional regimes obtained from the inversion of the fault–slip data and the earthquake focal mechanisms are mutually consistent with the convergence between the Afro–Arabian continent and the Eurasian continent.
- In the study area within the Zagros Foreland Folded Belt (F-FOB), a comparison between the paleo-compression directions obtained from fault–slip data and recent com-

pression directions obtained from earthquake focal mechanisms indicate that there was insignificant variation in the compression direction throughout time. However, an anticlockwise rotation in the direction of the principal compressional stress over time is compatible with the variation of Afro–Arabian and Eurasian continental collision paths. However, the NW compression direction observed in the middle segment of the Kar-e-Bass fault is incompatible with an anticlockwise rotation.

- The compatibility of our results with those of Lacombe et al. (2006) and Navabpour et al. (2007) (Fig. 18) indicates that there is not a significant difference in the compression direction in the vicinity of the lateral fault zones compared to the other parts of the Zagros orogenic belt. Consequently, the lateral fault zones (Kar-e-Bass, Sabz-Pushan, and Sarvestan fault zones) may have initiated as tear faults in the cover above the décollement horizon along the thrust (e.g., HZF and MFF), and in recent times, these fault zones act as strike–slip/dip–slip faults in both the basement and the sedimentary cover.
- The obliquity of the maximum principal stress into the fault trends reveals a typical stress partitioning of dip–slip and strike–slip motions in the Kazerun, Kar-e-Bass, Sabz-Pushan, and Sarvestan fault zones that caused these fault zones behave as segmented strike–slip/dip–slip faults.
- The almost relative consistency in the compressional direction in both the sedimentary cover and the gneissic basement suggests that there is no significant change in the crustal compressional trend between basement and cover.
- There are two sources of the fault activities either as pre-existing dip-seated reactivated faults or as shallow-seated faults of the decoupling or décollement of rheological weak evaporates in the study area.

References

Alavi M (1994) Tectonics of the Zagros orogenic belt of Iran: new data and interpretations. Tectonophysics 229:211–238

Allen MB, Saville C, Blanc EJP, Talebian M, Nissen E (2013) Orogenic plateau growth: Expansion of the Turkish–Iranian Plateau across the Zagros fold-and-thrust belt. Tectonics 32:1–20

Ambraseys NN (2001) Reassessment of earthquakes, 1900–1999, in the Eastern Mediterranean and the Middle East. Geophys J Int 145(2):471–485

Anderson EM (1951) The dynamic of faulting, 2nd edn. Edinburgh, Oliver and Boyd, p 133147

Angelier J (1979) Determination of the mean principal directions of stresses for a given fault population. Tectonophysics 56(3–4):T17–T26

Angelier J (1990) Inversion of field data in fault tectonics to obtain the regional stress—III. A new rapid direct inversion method by analytical means. Geophys J Int 103:363–376

Angelier J (1991) Chronological matrix analysis and regional succession of tectonic events. C R Acad Sci Paris t 312(Série II):1633–1638

Angelier J (1994) Paleostress determinations. In: Hancock PL (ed) Continental deformations. Pergamon Press, Tarrytown, NY, pp 53–100

Angelier J (2002) Inversion of earthquake focal mechanisms to obtain the seismotectonic stress IV—a new method free of choice among nodal planes. Geophys J Int 150:588–609

Aubourg C, Smith B, Eshraghi A, Lacombe O, Authemayou C, Amrouch K, Bellier O, Mouthereau F (2010) New magnetic fabric data and their comparison with stress/strain markers from the Western Fars arc (Zagros); tectonic implications. In Tectonic and Stratigraphic evolution of Zagros and Makran during the Meso-Cenozoic. Geol Soc Lond Spec Publ 330:97–120

Authemayou C, Bellier O, Chardon D, Malekzade Z, Abassi M (2005) Role of the Kazerun fault system in active deformation of the Zagros fold and- thrust belt (Iran). C R Geosci 337:539–545

Bayer R, Chery J, Tatar M, Vernant P, Abbassi M, Masson F, Nilforoushan F, Doerflinger E, Regard V, Bellier O (2003) Active deformation in Zagros—Makran transition zone inferred from GPS measurements. In: Fourth International Conference of Earthquake Engineering and Seismology, Tehran, Iran

Berberian M (1995) Master blind thrust faults hidden under the Zagros folds: active basement tectonics and surface tectonics surface morphotectonics. Tectonophysics 241:193–224

Berberian M, King GCP (1981) Towards a paleogeography and tectonic evolution of Iran. Can J Earth Sci 18:210–265

Bott MHP (1959) The mechanisms of oblique-slip faulting. Geol Mag 96:109–117

Burberry CM, Jackson C, Cosgrove JW (2011) Late Cretaceous to recent deformation related to inherited structures and subsequent compression within the Persian Gulf: a 2D seismic case study. J Geol Soc 168(2):485–498

Casciello E, Verges J, Saura E, Casini G, Fernandez N, Blanc E, Homke S, Hunt D (2009) Fold patterns and multilayer rheology of the Lurestan Province, Zagros simply folded belt (Iran). J Geol Soc Lond 166:1–13

Casini G, Gillespie PA, Vergés J, Romaire I, Fernández N, Casciello E, Saura E, Mehl C, Homke S, Embry JC, Aghajari L, Hunt DW (2011) Sub-seismic fractures in foreland fold and thrust belts: insight from the Lurestan Province, Zagros Mountains, Iran. Pet Geosci 17:263–282

Colman SP (1978) Fold development in Zagros simply folded belt, Southwest Iran. Am Assoc Pet Geol Bull 62(6b):984–1003

Cotton JT, Koyi HA (2000) Modelling of thrust fronts above ductile and frictional detachments: application to structures in the salt range and Potwar Plateau, Pakistan. Geol Soc Am Bull 112:351–363

Coward MP (1983) The thrust and shear zones of the Moine thrust zone and the NW Scottish Caledonides. J Geol Soc 140:795–811

Dasgupta S, Mukherjee S (2017) Brittle shear tectonics in a narrow continental rift: asymmetric non-volcanic Barmer basin (Rajasthan, India). J Geol

DeMets C, Gordon RG, Argus DF, Stein S (1990) Current plate motions. Geophys J Int 101:425–478

Doblas M (1998) Slickenside kinematic indicators. Tectonophysics 295:187–197

Engdahl R, van der Hilst R, Buland R (1998) Global teleseismic earthquake relocation with improved travel times and procedures for depth determination. Bull Seismol Soc Am 88:722–743

Falcon NL (1961) Major earth-flexuring in the Zagros Mountains of southwest Iran. Q J Geol Soc Lond 117:367–376

Falcon N (1974) Zagros Mountains, Mesozoic-Cenozoic orogenic belts. In: Spencer AM (ed) Mesozoic Cenozoic Orogenic Belts: Data for Orogenic Studies, collated, vol 4. Geological Society. Special Publications, London, pp 199–211

Farzipour-Saein A, Yassaghi A, Sherkati S, Koyi H (2009) Mechanical stratigraphy and folding style of the Lurestan region in the Zagros Fold–Thrust Belt, Iran. J Geol Soc 166:1101–1115

Fossen H (2016) Structural geology, 2nd edn. Cambridge University Press, New York, pp 1–463

GCMT Global Centroid Moment Tensor, Harvard University

Hatzfeld D (1999) The present-day tectonics of the Aegean as deduced from seismicity. Geol Soc Lond Spec Publ 156(1):415–426

Hatzfeld D, Authemayou C, Van der Beek P, Bellier O, Lavé J, Oveisi B, Tatar M, Tavakoli F, Walpersdorf A, Yamini-Fard F (2010) The kinematics of the Zagros Mountains (Iran). In: Leturmy P, Robin C (eds) Tectonic and stratigraphic evolution of Zagros and Makran during the Mesozoic-Cenozoic, vol 330. Geological Society, Special Publications, London, pp 19–42

Hessami K, Koyi HA, Talbot CJ, Tabasi H, Shabanian E (2001) Progressive unconformities within an evolving foreland fold–thrust belt, Zagros Mountains. J Geol Soc Lond 158:969–981

Hessami K, Jamali F, Tabassi H (2003) Major active faults of Iran (map). International Institute of Earthquake Engineering and Seismology

Hessami K, Nilforoushan F, Talbot CJ (2006) Active deformation within the Zagros Mountains deduced from GPS measurements. J Geol Soc Lond 163:143–148

Hippolyte JC, Bergerat F, Gordon MB, Bellier O, Espurt N (2012) Keys and pitfalls in mesoscale fault analysis and paleostress reconstructions, the use of Angelier's methods. Tectonophysics 581:144–162

Homke S, Verges J, Garces M, Emami H, Karpuz R (2004) Magnetostratigraphy of Miocene–Pliocene Zagros foreland deposits in the front of the Pusht-e Kuh Arc (Lurestan Province, Iran). Earth Planet Sci Lett 225:397–410

Huber H (1977) Geological map of Iran, 1:1,000,000 with explanatory note. National Iranian Oil Company. Exploration and Production Affairs, Tehran

Jackson J, McKenzie D (1984) Active tectonics of the Alpine-Himalayan belt between western Turkey and Pakistan. Geophys J R Astron Soc 64:561–586

Kaplay RD, Kumar TV, Mukherjee S, Wesanekar PR, Babar MD, Chavan S (2017) EW strike slip shearing of Kinwat Granitoid at South East Deccan Volcanic Province, Kinwat, Maharashtra, India. J Earth Syst Sci doi:10.1007/s12040-017-0853-8

Lacombe O (2012) Do fault slip data inversions actually yield paleostresses that can be compared with contemporary stresses? A critical discussion. C R Geosci 344:159–173

Lacombe O, Mouthereau F, Kargar S, Meyer B (2006) Late Cenozoic and modern stress fields in the western Fars (Iran): implications for the tectonic and kinematic evolution of central Zagros. Tectonics 25:TC1003

Lacombe O, Bellahsen N, Mouthereau F (2011) Fracture patterns in the Zagros Simply Folded Belt (Fars, Iran): constraints on early collisional tectonic history and role of basement faults. Geol Mag 148(5–6):940–963

Letouzey J, Sherkati S (2004) Salt movement, tectonic events and structural style, in the central Zagros fold and thrust belt, Iran.

6th Middle East Geosciences Conference, GEO. GeoArabia 9(1):96 **(abstract)**

Lohman RB, Simons S (2005) Locations of selected small earthquakes in the Zagros mountains. Geochem Geophys Geosyst Electron J Earth Sci 6:1–10

Maggi A, Jackson JA, Priestley K, Baker C (2000) A re-assessment of focal depth distributions in southern Iran, the Tien Shan and northern India: do earthquakes really occur in the continental mantle? Geophys J Int 143:629–661

Maggi A, Priastley K, Jacson J (2002) Focal depths of moderate and large size earthquakes in Iran. J Seismol Earthq Eng 4:1–10

McGarr A, Gay NC (1978) State of stress in the earth's crust. Annu Rev Earth Planet Sci 6:405–436

McKenzie DP (1969) The relation between fault plane solutions for earthquakes and the directions of the principal stresses. Bull Seismol Soc Am 59:591–601

McQuarrie N, Stock JM, Verdel C, Wernicke BP (2003) Cenozoic evolution of Neotethys and implications for the causes of plate motions. Geophys Res Lett 30(20):SDE6.1–SDE6.4

Misra AA, Mukherjee S (2017) Dyke–brittle shear relationships in the Western Deccan Strike slip Zone around Mumbai (Maharashtra, India). In: Mukherjee S, Misra AA, Calvès G, Nemčok M (eds) Tectonics of the Deccan large igneous province, vol 445. Geological Society, Special Publications, London, pp 269–295

Misra AA, Bhattacharya G, Mukherjee S, Bose N (2014) Near N–S paleo-extension in the western Deccan region in India: does it link strike-slip tectonics with India–Seychelles rifting? Int J Earth Sci 103:1645–1680

Molinaro M, Leturmy P, Guezou JC, Frizon de Lamotte D, Eshraghi SA (2005) The structure and kinematics of the southeastern Zagros foldthrust belt, Iran: from thin-skinned to thick-skinned tectonics. Tectonics 24:TC3007. doi:10.1029/2004TC001633

Motiei H (1993) Geology of Iran: stratigraphy of Zagros. Geological Survey of Iran, Persian, p 536

Mukherjee S (2011) Estimating the viscosity of rock bodies-a comparison between the Hormuz-and the Namakdan Salt Domes in the Persian Gulf, and the Tso Morari Gneiss Dome in the Himalaya. Indian J Geophys Union 15:161–170

Mukherjee S (2013) Channel flow extrusion model to constrain dynamic viscosity and Prandtl number of the Higher Himalayan Shear Zone. Int J Earth Sci 102:1811–1835

Mukherjee S (2014) Atlas of shear zone structures in meso-scale. Springer, New York, pp 1–124

Mukherjee S (2015a) A review on out-of-sequence deformation in the Himalaya. In: Mukherjee S, Carosi R, van der Beek P, Mukherjee BK, Robinson D (eds) Tectonics of the Himalaya, vol 412. Geological Society, Special Publications, London, pp 67–109

Mukherjee S (2015b) Atlas of structural geology. Elsevier, Amsterdam, pp 1–200

Mukherjee S, Talbot CJ, Koyi HA (2010) Viscosity estimates of salt in the Hormuz and Namakdan salt diapirs, Persian Gulf. Geol Mag 147:497–507

Mukherjee S, Koyi HA, Talbot CJ (2012) Implications of channel flow analogue models in extrusion of the Higher Himalayan Shear Zone with special reference to the out-of-sequence thrusting. Int J Earth Sci 101:253–272

Navabpour P, Angelier J, Barrier E (2007) Cenozoic post-collisional brittle tectonic history and stress reorientation in the High Zagros Belt (Iran, Fars Province). Tectonophysics 432:101–131

Ni J, Barazangi M (1986) Seismotectonics of the Zagros continental collision zone and a comparison with the Himalayas. J Geophys Res 91:8205–8218

Nissen E, Tatar M, Jackson JA, Allen MB (2011) New views on earthquake faulting in the Zagros fold-and-thrust belt of Iran. Geophys J Int 186(3):928–944

O'brien CAE (1950) Tectonic problems of the oil field belt of southwest Iran. In: Buiter J (eds), Proceedings of 18th International Geological Congress, Great Britain, Part 6, 45–58

Otsubo M, Sato K, Yamaji A (2006) Computerized identification of stress tensors determined from heterogeneous fault-slip data by combining the multiple inverse method and k-means clustering. J Struct Geol 28:991–997

Otsubo M, Yamaji A, Kubo A (2008) Determination of stresses from heterogeneous focal mechanism data: an adaptation of the multiple inverse method. Tectonophysics 457:150–160

Oveisi B, Lavé J, Beek P (2007) Rates and processes of active folding evidenced by Pleistocene terraces at the Central Zagros Front (Iran). Thrust belts and foreland basins frontiers in earth sciences, part V. Springer, Heidelberg, pp 267–287

Oveisi B, Lavé J, Beek P, Carcaillet J, Benedetti L, Aubourg C (2009) Thick- and thin-skinned deformation rates in the central Zagros simple folded zone (Iran) indicated by displacement of geomorphic surfaces. Geophys J Int 176:627–654

Ramsay JG, Huber MI (1987) The techniques of modern structural geology: folds and fractures, vol 2. Academic Press, London, p 700

Sarkarinejad K, Azizi A (2008) Slip partitioning and inclined dextral transpression along the Zagros thrust system, Iran. J Struct Geol 30:116–136

Sarkarinejad K, Ghanbarian MA (2014) The Zagros hinterland fold-and-thrust belt in-sequence thrusting, Iran. J Asian Earth Sci 85:66–79

Sarkarinejad K, Zafarmand B (2017a) Tectonic stress and kinematic analyses of the Ghir fault zone, Zagros, Iran. Persian Geosci 26(102):185–196

Sarkarinejad K, Zafarmand B (2017b) Stress state and movement potential of the Kar-e-Bas fault zone, Fars, Iran. J Geophys Eng 14:998–1009. doi:10.1088/1742-2140/aa6f2f

Sepehr M, Cosgrove JW (2004) Structural framework of the Zagros fold-thrust belt, Iran. Mar Pet Geol 21:829–843

Sepehr M, Cosgrove JW (2005) Role of the Kazerun Fault Zone in the formation and deformation of the Zagros fold-thrust belt, Iran. Tectonics 24:TC5005. doi:10.1029/2004TC001725

Sherkati S, Letouzey J (2004) Variation of structural style and basin evolution in the central Zagros (Izeh zone and Dezful embayment): Iran. Mar Pet Geol 21:535–554

Sperner B, Zweigel P (2010) A plea for more caution in fault–slip analysis. Tectonophysics 482:29–41

Stampfli GM, Borel GD (2002) A plate tectonic model for the Paleozoic and Mesozoic constrained by dynamic plate boundaries and restored synthetic oceanic isochrons. Earth Planet Sci Lett 196:17–33

Stöcklin J (1968) Structural history and tectonics of Iran: a review. Am Assoc Pet Geol 52:1229–1258

Stöcklin J (1974) Possible ancient continental margins in Iran. In: Burk CA, Drake CL (eds) Geology of continental margins. Springer, New York, pp 873–877

Stöcklin J, Nabavi MH (1973) Tectonic map of Iran. Geol Surv Iran 1:2500000

Talebian M, Jackson JA (2004) A reappraisal of earthquake focal mechanisms and active shortening in the Zagros mountains of Iran. Geophys J Int 156:506–526

Tatar M, Hatzfeld D, Martinod J, Walpersdorf A, Ghafori-Ashtiany M, Chéry J (2002) The present-day deformation of the central Zagros from GPS measurements. Geophys Res Lett 29:331–334

Tatar M, Hatzfeld D, Ghafori-Ashtiany M (2004) Tectonics of the central Zagros (Iran) deduced from microearthquakes seismicity. Geophys J Int 156:255–266

Tavakoli F, Walpersdorf A, Authemayou C, Nankali HR, Hatzfeld D, Tatar M, Djamour Y, Nilforoushan F, Cotte N (2008)

Distribution of the right-lateral strike–slip motion from the main recent fault to the Kazerun Fault System (Zagros, Iran): evidence from present-day GPS velocities. Earth Planet Sci Lett 276:342–347

Twiss RJ, Unruh JR (1998) Analysis of fault slip inversions: do they constrain stress or strain rate? J Geophys Res 103:12205–12222

Vernant Ph, Nilforoushan F, Hatzfeld D, Abbassi MR, Vigny C, Masson F, Nankali H, Martinod J, Ashtiani A, Bayer R, Tavakoli F, Chéry J (2004) Present-day crustal deformation and plate kinematics in the Middle East constrained by GPS measurements in Iran and northern Oman. Geophys J Int 157:381–398

Wallace RE (1951) Geometry of shearing stress and relation to faulting. J Geol 59:118–130

Walpersdorf A, Hatzfeld D, Nankali H, Tavakoli F, Nilforoushan F, Tatar M, Vernant P, Chery J, Masson F (2006) Difference in the GPS deformation pattern of north and central Zagros (Iran). Geophys J Int 167:1077–1088

Yamaji A (2000a) Multiple inverse method applied to mesoscale faults in mid Quaternary sediments near the triple trench junction off central Japan. J Struct Geol 22:429–440

Yamaji A (2000b) The multiple inverse method: a new technique to separate stresses from heterogeneous fault-slip data. J Struct Geol 22:441–452

Yamaji A, Tomita S, Otsubo M (2005) Bedding tilt test for paleostress analysis. J Struct Geol 27:161–170

Yamaji A, Sato K, Otsubo M (2011) Multiple inverse method software package. User's guide 1–37

Yamini-Fard F, Hatzfeld D, Tatar M, Mokhtari M (2006) Microseismicity at the intersection between the Kazerun fault and the Main Recent Fault (Zagros-Iran). Geophys J Int 166:186–196

Yamini-Fard F, Hatzfeld D, Farahbod A, Paul A, Mokhtari M (2007) The diffuse transition between the Zagros continental collision and the Makran oceanic subduction (Iran): microearthquake seismicity and crustal structure. Geophys J Int 170:182–194

Zalohar J, Vrabec M (2007) Paleostress analysis of heterogeneous fault slip data: the Gauss method. J Struct Geol 29(11):1798–1810

Ziegler PA, Bertotti G, Cloetingh S (2002) Dynamic processes controlling foreland development: role of mechanical (de)coupling of orogenic wedges and foreland. EGU Stephan Mueller Special Publication Series 1, pp 17–56

ZUR-RMT Zurich Moment Tensor. Swiss Seismological Service